The role of inhibitory neurons in novelty sound detection in regular and random statistical contexts.

Abbreviated title: Inhibition controls novelty context dependence

Xiaomao Ding[1,2], Nathan W. Vogler[1], Melanie Tobin[1], Linda Garami[1], Katherine C. Wood[1,3], Maria N. Geffen[1,2]

1. Department of Otorhinolaryngology, University of Pennsylvania, Philadelphia, PA, USA

2. Neuroscience Graduate Group, University of Pennsylvania, Philadelphia, PA, USA

3. University of Sheffield, Sheffield UK

*Corresponding author:
Maria Neimark Geffen, Ph.D. (she/her)
Department of Otorhinolaryngology
Perelman School of Medicine
University of Pennsylvania
5 Ravdin
3400 Spruce St.
Philadelphia PA 19104
Tel.: 215.898.0782

Number of pages: 49

Number of figures: 8 main figures + 3 supplemental figures

Conflict of Interest: The authors declare no conflicts of interest in collecting and analyzing the data and preparing this manuscript.

Acknowledgements

The authors would like to thank the members of the Geffen laboratory and Yale Cohen for their discussions and helpful comments. This work was supported by the following grants from NIDCD: R01DC15527, R01DC014479, R03DC013660, NINDS R01NS113241 to MNG, and K99DC019504 to KCW. XD was supported by T32DC016903.

ABSTRACT

Detecting statistical regularities in sound and responding to violations of these patterns, termed novelty detection, is a core function of the auditory system. In the human brain, studies have shown that novelty responses are enhanced in regular compared to random auditory contexts, but the underlying neuronal circuit mechanisms remain unclear. Here, we examined how inhibitory neurons contribute to context-dependent novelty responses in mouse auditory cortex (AC). Using two-photon calcium imaging in AC of awake head-fixed male and female mice, we recorded neuronal activity during presentation of spectro-temporally rich ripple sounds, with novel ripples embedded in either regular or random ripple sequences. AC neurons exhibited stronger responses to novel sounds in regular contexts compared to random ones. To identify circuit mechanisms, we selectively inactivated parvalbumin (PV), somatostatin (SST), or vasoactive intestinal polypeptide (VIP) inhibitory neurons during the novel stimulus presentation. Inactivation of PV and SST neurons broadly increased novelty responses in both contexts. In contrast, VIP inactivation selectively reduced responses to novel stimuli in the regular, but not random, context, decreasing the context-dependent novelty signal enhancement. At the population level, inactivating all three neuronal subtypes increased detectability of the novel stimulus, but only for VIP inactivation, the effects were context dependent. These findings reveal a distinct role for VIP neurons in modulating novelty signals based on context regularity, suggesting that VIP circuits are critical for context-sensitive auditory processing and predictive coding.

SIGNIFICANCE STATEMENT

Understanding how the brain detects and responds to predictable and unexpected sounds is critical for communication and navigation in complex acoustic environments. Although prior studies have shown that detection of novel sounds is enhanced by regularity in background sound patterns, the underlying circuit mechanisms have remained unknown. Here, we find that neurons in the auditory cortex exhibit stronger novelty responses to novel sounds embedded in regular, predictable sound sequences as compared to random sound sequences. Importantly, we identify a distinct role for specific inhibitory neurons in modulating this context-dependent enhancement. These findings reveal a new insight into how cortical circuits implement predictive coding strategies to optimize sensory processing.

INTRODUCTION

Successfully navigating everyday sound environments requires the auditory system to detect and interpret unexpected sounds within predictable patterns (Barascud et al., 2016; Sohoglu and Chait, 2016; Parras et al., 2017; Southwell and Chait, 2018). Natural sounds are characterized not only by their spectral content but also by higher-order spectro-temporal regularities: statistical relations that allow listeners to form predictions about upcoming auditory events. Detecting violations of these predictions—referred to as *novelty detection*—is a core auditory computation. These computations support a wide range of behaviors, from identifying a familiar voice in a noisy crowd to detecting an approaching vehicle amid ambient noise (Arnal and Giraud, 2012). Extensive research in humans and non-human animals has demonstrated that the brain encodes both predictions and prediction errors, with signals such as the mismatch negativity (MMN) reflecting changes in neural activity in response to unexpected sounds (Naatanen et al., 1978, 2004,

2007). Novelty signals have been observed across multiple stages of the auditory pathway, including the inferior colliculus (IC) (Lesicko et al., 2022), medial geniculate body (MGB) (Antunes et al., 2010; Malmierca et al., 2015), and auditory cortex (AC) (Nelken, 2004, 2014; Hershenhoren et al., 2014; Natan et al., 2015, 2017; Rubin et al., 2016; Parras et al., 2017). However, the transformations of prediction and deviance signals along this pathway, and the neural mechanisms that shape their context sensitivity, remain incompletely understood.

Recent studies in humans have shown that novelty responses are enhanced when novel sounds are embedded within regular, predictable contexts as compared to random ones (Sohoglu and Chait, 2016; Southwell and Chait, 2018). For example, a regular context may consist of a repeating sound sequence (e.g., ABCD, ABCD…), whereas a random context involves the same elements shuffled in order (e.g., BADC, ADCB…). Stronger responses to a novel sound X following a regular pattern suggest that the brain not only detects violations in the global structure of sound, but also modulates prediction strength based on contextual, local structure. Whereas EEG studies point to AC as the center for the context-dependent novelty responses, how these responses are created at individual neuronal and circuit levels remains unknown. Nearly all neurons in AC show adaptation to frequently presented sounds and an enhanced response to rare, deviant stimuli (Harms et al., 2014; Parras et al., 2017) — a phenomenon known as stimulus-specific adaptation (SSA) (Ulanovsky et al., 2003; Szymanski et al., 2009; Farley et al., 2010; Natan et al., 2015). Furthermore, studies have shown that AC neurons are also sensitive to patterns with structure across multiple time scales (Ulanovsky et al., 2004; Yaron et al., 2012; Mehra et al., 2022). Here, we asked whether individual AC neurons exhibit enhanced novelty responses in regular as compared to random context, and whether intra-cortical inhibitory-excitatory circuits support this transformation.

Inhibitory neurons in AC play distinct roles in shaping auditory cortical responses to sound patterns. The two most common subtypes, parvalbumin (PV)- and somatostatin (SST)-expressing neurons (Lee et al., 2010; Tremblay et al., 2016; Wood et al., 2017), differentially contribute to SSA and other forms of auditory adaptation (Levy and Reyes, 2012; Chen et al., 2015; Natan et al., 2015, 2017; Phillips et al., 2017), while another prominent subtype, vasoactive intestinal polypeptide (VIP)-expressing neurons, contribute to context- and state-dependent modulation in multiple cortical areas (Lee et al., 2010; Tremblay et al., 2016; Wood et al., 2017). VIP neurons in particular have been proposed to gate top-down influences and modulate predictive coding processes through a disinhibitory circuit. We hypothesized that these distinct inhibitory neuron classes differentially contribute to novelty detection depending on regular or random context.

Using two-photon calcium imaging in awake mice, we recorded neuronal activity of large populations of neurons in auditory cortex during presentation of novel spectro-temporally complex ripple stimuli embedded in either regular or random sound contexts. We combined imaging with optogenetic inactivation of PV, SST, or VIP neurons to determine their respective roles in modulating novelty responses. We found that regular context enhanced novelty responses compared to random context, and that this enhancement was differentially shaped by inhibitory neuron class. PV and SST inactivation increased responses to novel sounds, but the role of context was non-specific, whereas VIP inactivation selectively reduced novelty responses in the regular, but not random context. These results identify VIP neurons as a key component of the circuit that integrates context statistics to shape novelty responses.

METHODS

Animals

124 A total of 14 mice (male/female) were used in this study. The strains used were: Cdh23 x PV-Cre
125 (B6.CAST-Cdh23Ahl+/Kjn, JAX: 002756 x Pvalbtm1(cre)Arbr/J, JAX: 017320; n = 4),
126 Cdh23xSST-Cre (B6.CAST-Cdh23Ahl+/Kjn x Ssttm2.1(cre)Zjh/J, 113 JAX: 013044; n = 4), VIP-
127 IRES-Cre (B6.CAST-Cdh23Ahl+/Kjn x Viptm1(cre)Zjh/J, JAX: 010908; n = 3), VGAT-Cre
128 crossed with transgenic GCaMP8m (Slc32a1tm2(cre)Lowl/J, JAX: 016962 x Igs7tm1(tetO-
129 GCaMP8m,CAG-tTA2)Genie/J, JAX:037718, n = 3), Cdh23 (B6N(Cg)-Cdh23tm2.1Kjn/Kjn, n =
130 5), aged 12-26 weeks. Cdh23 mice were used because they do not exhibit age-related hearing loss
131 which is common in C57BL/6J mice (Johnson et al., 2017). Mice were housed individually after
132 cranial window implant and were housed on a reversed light-dark cycle. Experimental procedures
133 were performed in accordance with NIH guidelines and approved by the IACUC at the University
134 of Pennsylvania.
135

136 **Surgery Procedures**

137 Cranial window implants were implanted following a procedure described previously (Wood et
138 al., 2022; Tobin et al., 2024). Mice were anesthetized with 3% isoflurane which was steadily
139 reduced to 1.5% through the surgery. A 3 mm craniotomy was performed over the left auditory
140 cortex with a 3 mm biopsy punch. A viral 750 nL cocktail (4:1 ratio) of virus encoding GCAMP
141 (7f: AAV1-Syn-jGCaMP7f-WPRE, Addgene 104488 or 8m: pGP-AAV-syn-jGCaMP8m-WPRE,
142 Addgene 162375) and virus encoding Jaws in a Cre-dependent fashion (AAV8-CAG-FLEX-
143 JAWS-kgc-tdTomato, UNC Vector Core or AAV8-CAG-FLEX-JAWS-kgc-tdTomato, Penn Vector
144 Core, Addgene 84446) was injected at 3 locations in the craniotomy, separated 0.3-0.5 mm apart
145 in the anterior-posterior direction. The craniotomy was then sealed with a custom round glass
146 window consisting of a 3 mm window glued to a 4 mm window with Norland Optical Adhesive

68. A custom-made metal headplate was attached to the skull with C&B Metabond dental cement. For transgenic GCaMP8m mice, no virus was injected and only the window implant was performed. Mice were allowed to recover for 3 weeks before imaging started.

Two-photon imaging

All imaging sessions were performed in a custom-built acoustic isolation booth using previously published methods (Betzel et al., 2019; Wood et al., 2022; Tobin et al., 2024). Mice were habituated to being head fixed for 3 days prior to imaging. Wide-field imaging was performed on each mouse to identify sound-responsive areas of the window before two-photon imaging. We imaged in layer 2/3 of auditory cortex of awake head-fixed mice using a two-photon (2P) microscope (Ultima 2Pplus *in vivo* multiphoton microscope, Bruker) with a 940 nm laser (Chameleon Ti-Sapphire) with a 16X Nikon objective with a 0.8 numerical aperture (Thorlabs, N16XLWD-PF) (Figure 1 A, B, D). Recordings were made at 512 x 512 pixels and at 30 frames per second.

Optogenetic Manipulation

Optogenetic stimulation was performed using a LED (Thorlabs M625L4) delivering 625 nm light through the objective lens (Tobin et al., 2024). Before each stimulus session, the LED light power was calibrated to ~2.8 mW/mm^2 for mice injected with the virus encoding Jaws from the Penn Vector Core and ~7 mW/mm^2 for mice injected with the virus encoding Jaws from the UNC Vector Core based on reported inhibition performance of Jaws (Chuong et al., 2014). Optogenetic manipulation occurred randomly in 50% of presentations of the novel ripple. The LED was turned on continuously for 300 ms, synced with stimulus onset, during the novel ripple presentation. Control mice (SST-Cre, n=2) were injected with the viruses encoding tdTomato (in a Cre-dependent fashion) and GCaMP, but not Jaws (Supplementary Figure 3), and exhibited a much weaker and inconsistent effect of light on tuning stimulus ripple responses.

Acoustic stimuli

Auditory moving ripples were generated at a sampling rate of 400 kHz in MATLAB according to the following formula:

$$S(t,x) = L[1 + \Delta A sin(2\pi wt + 2\pi\Omega x + \Phi)]$$

where w is the temporal modulation parameter and Ω is the spectral modulation parameter. Individual ripples spanned a frequency range of 5-50 kHz, lasted 300 ms, were presented at 70 dB SPL with a 15 dB modulation depth, and had a 5 ms cosine ramp applied at the beginning and end. Background sequences were generated by concatenating ripples A, B, C, and D in either a fixed sequence (REG) or a random sequence (RND) resulting in a 1.2 s stimulus (Figure 1C). The novel sequence was generated by concatenating ripples X, Y, Z, and W in that order for all stimulus conditions. Sequences were presented with a 1 s inter-stimulus interval. Background sequences were repeated 3-6 times pseudo-randomly before a novel sequence was presented. A control sequence of each ripple presented in isolation with a 1 s ISI was also presented to determine the base sound response of neurons.

Electrophysiology

Mice were prepared for *in vivo* electrophysiological recordings as described previously (Vogler et al., 2024). At least two weeks prior to recordings, a ground pin was inserted via small craniotomy over the left frontal cortex, and a custom-made stainless steel headplate (eMachine Shop) was secured to the skull using dental cement (C&B Metabond) and acrylic (Lang Dental) (Vogler et al., 2024). Recordings were performed in a custom-built acoustic isolation booth. At least one week following headplate surgery, mice were habituated to the recording setup for increasing durations (5-60 min) over the course of 3 days. On the day of recording, mice were anesthetized with 1.5-2.5% isoflurane, and a small craniotomy was made over the left auditory cortex using a

193 dental drill, centered ~1.5mm anterior to the lambdoid suture along the caudal end of the
194 squamosal suture. Following the craniotomy, mice were allowed to recover from anesthesia for at
195 least 30 min. Acute extracellular recordings in the auditory cortex were performed using a 32-
196 channel silicon probe (A1x32-Poly2-5mm-50s-177, NeuroNexus). The probe was positioned
197 perpendicularly to the brain surface and lowered at 1-2 μm/s to a final depth of 900-1200 μm or
198 until all channels were within the brain. During lowering of the probe, we monitored responses to
199 brief broadband noise clicks to confirm localization within auditory cortex. Neuronal signals were
200 amplified and digitized with an Intan headstage (RHD 32ch) and recorded by an OpenEphys
201 acquisition board (Siegle et al., 2017) at a rate of 30 kHz. Signals were filtered between 500 and
202 6000 Hz, offset corrected, and re-referenced to the median across all channels. Spiking data were
203 sorted using Kilosort2 (Pachitariu et al., 2016) and manually curated in phy2 to identify putative
204 single- and multi-units.

205 **Immunohistochemistry**

206 Mouse brains were extracted and sliced as previously reported (Wood et al., 2022; Vogler et al.,
207 2024). In brief, mice were anesthetized with an injection of dexmedetomidine (1 mg/kg) and
208 ketamine (120 mg/kg) and then perfused with phosphate-buffered saline (PBS) and 4%
209 paraformaldehyde (PFA). Brains were fixed in 4% PFA overnight at 4°C. Coronal slices were
210 acquired on a cryostat (Leica CM1860) at −25°C. Slices were incubated overnight at 4°C with an
211 RFP antibody (1:1000, Rockland: 600-401-379) followed by an anti-rabbit secondary for 2 hours
212 at room temperature before imaging (see representative images from VIP-Cre, PV-Cre and SST-
213 Cre mice of neurons labels with tdTomato and GCaMP in Supplementary Figure 1). Expression of
214 GCaMP was identified and cross-referenced with the Paxinos mouse brain atlas (Figure 1A
215 bottom).

Data analysis and statistics

Suite2P (Pachitariu et al., 2017) was used to register raw two-photon images, select regions of interest (ROI), and perform neuropil correction (Betzel et al., 2019; Wood et al., 2022; Tobin et al., 2024). A 0.3 Hz highpass filter was used to correct for slow fluctuations in the calcium signal. The calcium signal from each ripple sequence was converted to a z-scored $\Delta F/F_{std}$=(F-mean($F_{baseline}$))/std($F_{baseline}$) where $F_{baseline}$ is the calcium signal from the 300 ms preceding stimulus onset. An additional motion correction step was performed using PatchWarp (Hattori and Komiyama, 2022). We found that small motion artifacts during imaging induced negative transients in the calcium trace. These artifacts were identified by setting a threshold for the X and Y values from the summary stat output and any trials within 3 frames of an artifact were removed from further analysis. This removed approximately 10% of all trials recorded. For statistical comparison of responses, we computed the mean response strength during the 300 ms following the onset of a ripple on each trial. To identify neurons exhibiting significant novelty responses, we compared the responses over trials during the same ripple presented as novel and tuning stimulus using an unpaired t-test in either random or regular context. To compare novelty response strength across neurons in different conditions, we computed mean response to the first ripple X in the novel stimulus sequence and implemented repeated measures ANOVA with context (regular or random) and light (on or off) as two factors. We used Tukey-Kramer for post-hoc comparisons. If the output of the statistical test in MATLAB resulted in “p = 0”, this was most likely due to a rounding error and we reported it as $p < 1e\text{-}20$. The results from all statistical tests are reported in Table 1.

REGRND Index

The REGRND index was computed as the difference between the absolute values of the mean response to the novel ripple presented in the REG and RND contexts divided by the sum of the absolute values. This provides a value between -1 and 1 where an index value close to 1 indicates that the neuron preferred to respond to the REG context, a value close to -1 indicates a preference for RND, and a value close to 0 indicates no preference.

Exponential Fits

Mean responses y from 0-300 ms after stimulus onset for individual trials were fit to the exponential function below:

$$y = a * e^{bx} + c$$

The variables a, b, and c were free parameters, and the variable x represented the trial presentation number. A neuron was considered to have a significant adaptation effect ($a > 0$) or facilitation effect ($a < 0$) if the RMSE from the exponential fit was less than the RMSE to the mean response. Fits were performed using MATLAB's curve fitting toolbox.

SVM

Sample populations of neurons were selected by bootstrapping either 1, 12, 25, 50, 100, or 200 neurons from within a single recording session. For each sample, the population response was represented as a vector with each entry being the mean response of a neuron from 0-300 ms from stimulus onset for an individual trial. Then, a support vector machine (SVM) was trained to predict either ripple identity from the tuning stimulus or background context (REG/RND) from the novelty stimulus (Vapnik, 2013; Wood et al., 2022; Tobin et al., 2024). 20% of the trials were held out as a test set while the SVM was trained on the remaining 80%. For each population size, sample neuronal responses were bootstrapped 1000 times. Results presented represent the mean prediction performance across 1000 models for the specified population size.

RESULTS

Characterizing the sound response to individual moving ripples

We imaged calcium activity in populations of neurons in layer 2/3 of auditory cortex (AC) in awake, head-fixed mice presented with a series of sequences of spectro-temporally complex sounds (termed "ripples") (Figure 1 A-D). Each ripple was comprised of a broadband sound with the envelope and frequency modulation varying in time. For the regular (REG) and random (RND) background ripples, we used the same 4 ripples (300 ms long, 5-50 kHz, 70 dB SPL mean intensity), which were repeated in the same sequence (REG; ABCD, ABCD, ABCD, …), or in varying order (RND; BADC, BDAC, CBDA, …). Each background sequence consisted of 3-6 repeats of the 4 ripples with 1 s inter-repeat interval followed by the novel ripple sequence. Because the background sequence is comprised of the same ripples in both REG and RND, the only difference between the two contexts is the temporal order. The novel sequence of ripples included 4 different ripples from those used in the background. These ripples were in the same frequency range but had different modulation frequencies. Additionally, the ripples were also presented individually with a 1 sec interstimulus interval to construct baseline tuning responses.

This stimulus allowed us to test multiple aspects of the neuronal responses to sounds in varying statistical regimes. First, we tested whether a given ripple evoked a greater or smaller neuronal response when it was unexpected. Second, we tested whether a novel ripple elicited a greater or smaller response in the regular or random context. Third, we tested whether the responses to the context ripples differed when they were presented in regular or random context, and whether adaptation to their presentation over subsequent repeats differed based on whether their order was regular or random. We expected the responses to novel ripples to be greater than the respective baseline sound response. We also expected novelty responses to be greater in the

regular than random context. Finally, we expected adaptation to repeated ripple sequences to be stronger for regular than random contexts.

We recorded activity from 8,573 neurons in the AC, with 76.6% (n = 6,566) showing a significant sound response to at least one ripple (z-scored averaged fluorescent response 0-300 ms post stimulus-onset versus the average fluorescence 0-300 ms before stimulus on each trial, t-test with a Bonferroni correction for the number of ripples). The fluorescence of neurons typically increased over the first 200 ms after sound presentation followed by a gradual decrease in fluorescence (representative neurons, Figure 1E, F). Across all imaged neurons, 22.4% (n = 1,922/8,573) responded to only one ripple while 6.3% (n = 541/8,573) had significant responses to all eight ripples. Additionally, the distribution of responsive neurons by ripple was relatively even across all eight ripples, with a maximum difference in response rate of 22.4% (Figure 1G, H). Whereas many neurons exhibited an enhancement in fluorescence in response to the ripples (n = 1,967/6,566), the majority of imaged neurons exhibited a suppression in fluorescence to individual ripples (n = 4,599/6,566, Figure 1I). The suppression in fluorescence corresponds to a decrease in calcium concentration, which most likely is due to reduced spiking activity in response to the moving ripples (Attinger et al., 2017; Solyga and Keller, 2025). When appropriate, we analyzed the enhanced responses as a separate group from suppressed responses. Combined, responses to individual ripples demonstrate that these stimuli efficiently drive neuronal calcium responses in AC.

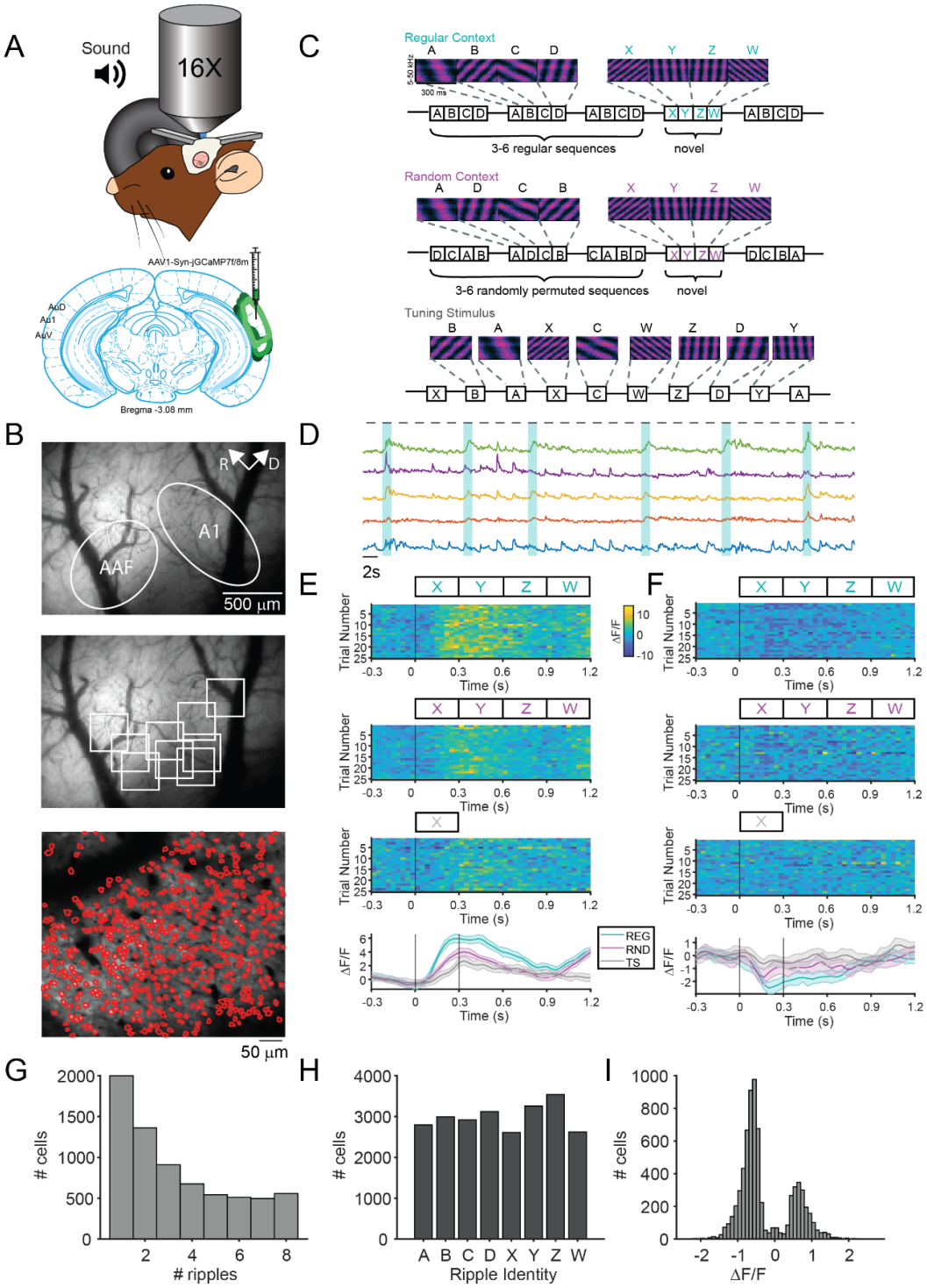

FIGURE 1

A. Schematic of two-photon (2P) calcium imaging setup (top), and viral spread across AC for GCaMP injections (bottom). **B.** Widefield image from an example mouse with identified areas for A1 and anterior auditory field (AAF) regions (top). Recording sites across different mice mapped onto the example widefield image (middle). Example 2P imaging site with ROIs circled in red

(bottom). **C.** Spectrograms of spectro-temporal moving ripples used in the experiment and stimulus schematic. Ripples spanned 5-50 kHz and were 300 ms long in duration. Regular sequences had a fixed temporal pattern (ABCD ABCD…) while random sequences shuffled the background ripple order (DCAB BACD…). The novel stimulus (novel) sequence was the same for both conditions (XYZW). Each letter in the diagram represents a different spectro-temporal moving ripple. **D.** Example 2P calcium traces from 5 neurons from the same recording session. Black bars on top denote the timing of each ripple sequence. Blue outlines denote the timing of novel ripple sequences. **E,F.** Responses over the successive trials (top 3 plots) and mean response trace (bottom) to the same novel ripple in regular (cyan) and random (magenta) contexts as well as the same ripple in the tuning sequence (gray) from example cells with a positive response (**E**) and a negative response (**F**). Shaded error bars represent SEM. **G.** Histogram of number of neurons responsive to only 1 ripple up to all 8 ripples. A significant response was determined with a t-test of the mean response from 0-300 ms post-stimulus a $p < 0.05$ with a Bonferroni correction. **H.** Histogram of number of neurons responsive to specific ripples. **I.** Histogram of number of mean baseline sound response amplitudes for all sound responsive neurons.

Regularity of context modulates novelty response

Most neurons in AC that we imaged exhibited a novelty response: 51.2% of neurons exhibited a stronger response to the novel ripple in either the RND or REG condition as compared to the tuning response (significant change in mean response within the 300 ms window post-stimulus onset to the novel ripple compared to tuning response to that ripple). There was a significant effect of novelty on the response to the same ripple (n = 4,391, repeated measures ANOVA, $f(2) = 51.18$, $p = 7.95e-23$). These changes in novelty responses were significant when computed separately for the positive (n = 2,429, repeated measures ANOVA, $f(2) = 1816.91$, $p < 1e-20$, Figure 2A-D) and negative (n = 1,962, repeated measures ANOVA, $f(2) = 1324$, $p < 1e-20$, Figure 2F, G, H) responding neurons. The remaining neurons (n = 4,182) exhibited no significant difference in response to the novel ripple compared to its baseline response (Figure 2J, K, L). Novelty responses were also significant for a group that included positive novelty responses as well as positive baseline responses (n = 191, repeated measures ANOVA, $f(2) = 129.72$, $p = 1.14e-43$, Figure 2N, O, P).

For positive novelty responses, the REG context enhanced the novelty response in the corresponding direction. The novelty response magnitude was greater under the REG context than under the RND context (49.5%, post-hoc Tukey-Kramer, p = 5.96e-08, Figure 2B, C, D). The context-dependent difference in novelty response strength persisted when we considered neurons with both positive novelty and baseline sound responses to the novel ripple (33.1%, post-hoc Tukey-Kramer, p = 5.96e-08, Figure 2N, O, P). For negative-responding neurons, the difference in novelty response between the REG and RND contexts was not significantly different (post-hoc Tukey-Kramer, p = 0.63, Figure 2G, H). Interestingly, neurons that did not exhibit significant novelty responses had a small preference for the REG context (post-hoc Tukey-Kramer, p = 0.032, Figure 2J, K, L). For positive novelty responses, these results are consistent with our predictions, as we expected the novelty response to be stronger in the regular compared to random conditions. Since negative responses are more difficult to interpret, the lack of difference in novelty responses across contexts may be due to averaging across multiple effects such as a suppression of negative activity, or switch from negative to positive responses between contexts.

To further understand the preference of individual neurons' novelty responses for temporal context, we computed a REGRND index (see Methods) which ranged from -1 to 1, with -1 indicating a preference for the RND context and 1 indicating a preference for the REG context. For positive novelty responses, we found that a majority of neurons only exhibited a significant novelty response in one of the REG (43.8%) or the RND (24.5%) contexts. For neurons exhibiting a significant novelty response in both contexts, we found a significant preference for the REG context when considering the REGRND index (mean = 0.06, t-test, p = 1.31e-10, Figure 2E). This preference for the REG context is even stronger when we only consider neurons with a positive novelty response and a positive baseline sound response (mean = 0.12, t-test, p =0.0046, Figure

2Q). On the other hand, negative novelty responses exhibit a small difference in the percentage of neurons selective for the REG (36.9%) and RND (30.8%) contexts and no significant difference in the REGRND index for neurons responsive in both (mean = 0.015, t-test, p = 0.14, Figure 2I). Thus, novelty responses are not only increased in their magnitude in the REG over RND contexts, but also in the fraction of responsive neurons.

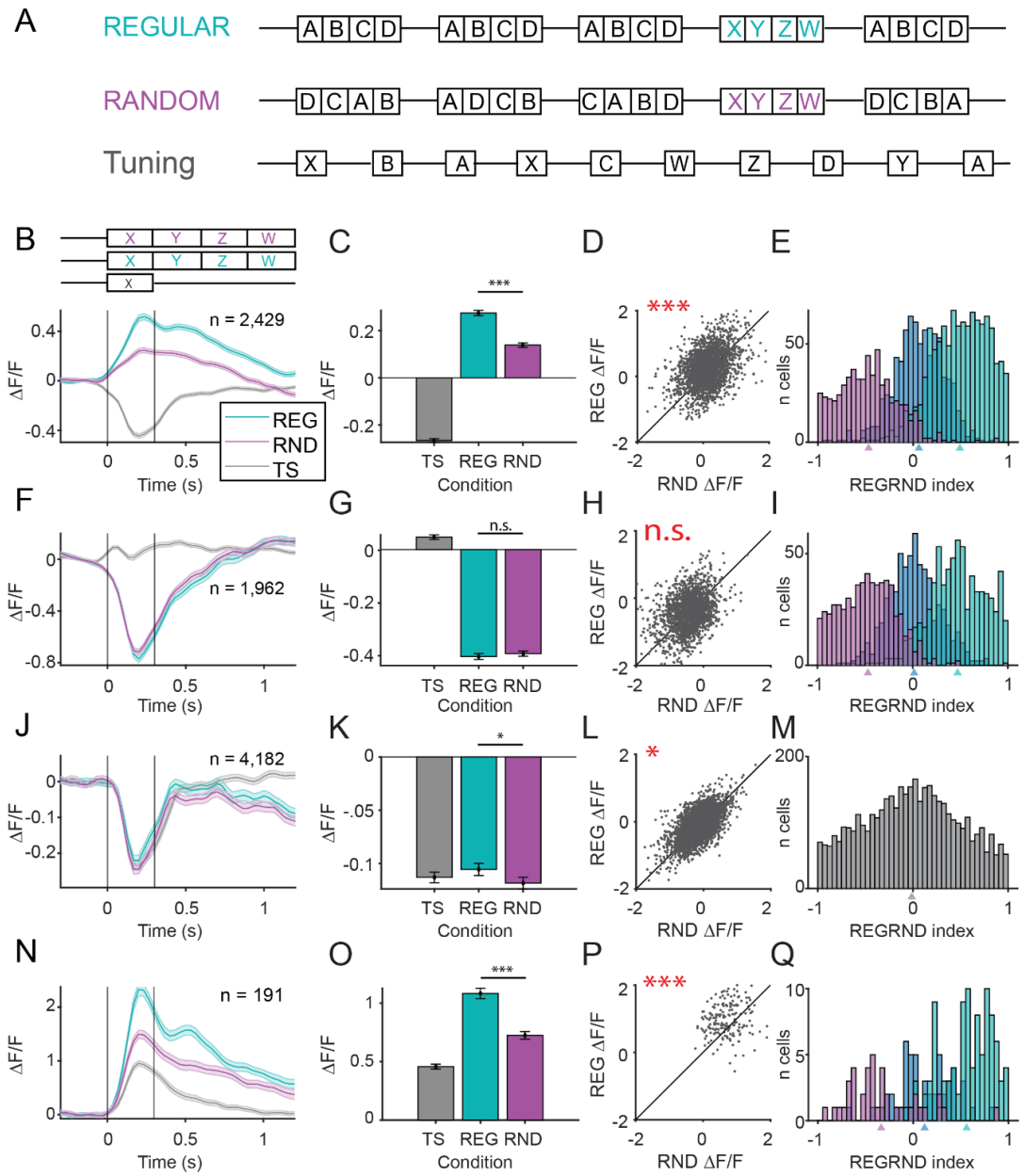

FIGURE 2

AC neurons exhibit stronger novelty responses in regular than random contexts.

A. Schematic of the stimuli for REG and RND contexts (sequence of 4 ripples ABCD) with novel ripples (XYZW). A tuning stimulus comprising each of 8 ripples was used to identify the baseline sound response to the ripples for individual neurons. **B.** Population-averaged calcium traces across neurons with positive novelty response to the novel ripple presented in the REG context (cyan), RND context (magenta), and as part of tuning stimulus (grey) as z-scored ΔF/F on the left. Vertical lines represent duration of the first novel ripple. **C.** Mean responses to the novel ripple over 300 ms post stimulus onset in REG, RND and tuning (TS) contexts. **D.** Scatter plot of responses to novel ripple under REG and RND contexts. **E.** Histogram of the REGRND index for responses to the novel ripple for neurons with preference for REG context (cyan), RND context (magenta) or no preferences (gray). Mean values for the index for each group are denoted by triangles below the x-axis. **B, C, D, E.** Responses of neurons that exhibit positive responses to novel ripple under either REG or RND contexts. The mean responses show a significant effect of context on the response amplitude (n = 2,429, repeated measures ANOVA: $p < 1e\text{-}20$) with novelty responses in REG context being the strongest (REG), followed by novelty responses in RND context (RND), and then the tuning stimulus responses (TS) (post-hoc Tukey-Kramer, p = 5.96e-08). **F, G, H, I.** Similar to B-E, but for responses of neurons that exhibit negative responses to novel ripples under either REG or RND context (n = 1,962, repeated measures ANOVA, $p < 1e\text{-}20$). For negative responses, there is no difference between REG and RND novelty responses (post-hoc Tukey-Kramer, p= 0.63). **J, K, L, M.** Similar to above, but for all neurons without a significant novelty response (n = 4,182, repeated measures ANOVA, p = 0. 023). While there was no significant difference between baseline and REG (post-hoc Tukey-Kramer, p = 0.21) or RND (post-hoc Tukey-Kramer, p = 0.46), there was a slight difference between REG and RND responses (post-hoc Tukey-Kramer, p = 0.032). **N, O, P, Q.** Similar to above, for all neurons with both a positive sound response and a positive novelty response (n = 191, repeated measures ANOVA, $p < 1e\text{-}20$). REG responses are the strongest, followed by RND responses, followed by TS responses (post-hoc Tukey-Kramer, p = 5.96e-8).

We next analyzed how the novelty response changes over the course of an entire REG or RND stimulus block. Previous work has shown that adaptation in AC occurs over multiple time scales (Ulanovsky et al., 2004). We hypothesized that temporal regularity may also impact adaptation on longer time scales in a similar manner, with stronger adaptation occurring in the REG context compared to the RND context. We fit an exponential response function to the time course of per trial responses from individual neurons (Figure 3A, B, E). We found that a sizeable fraction of neurons exhibited long term adaptation (48.03%) or facilitation (41.52%) to the novel ripple presentation. Neurons adapted or facilitated faster in the REG as compared to RND context

(Figure 3C, D, F, G): time constants for both adaptation and facilitation were greater in the RND context than the REG context ($n_{adapt\ REG}$ = 2,545, $n_{facil\ REG}$ = 2,032, $n_{adapt\ RND}$ = 2,224, $n_{facil\ RND}$ = 1,843, 2-way ANOVA, f(1) = 10.29, p = 0.0044), indicating that context has a secondary effect on the long-term adaptation of neuronal responses to the novel ripple. These results demonstrate a secondary mechanism for adaptation to stimulus context during novelty detection.

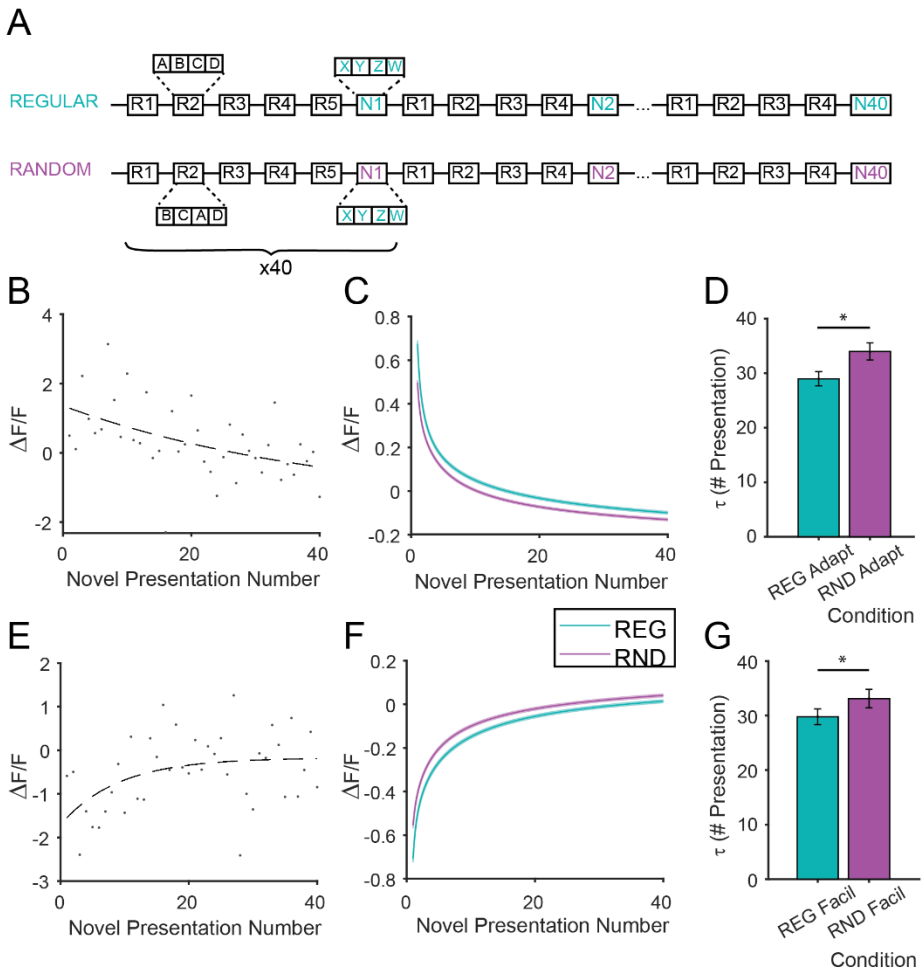

Figure 3

Temporal regularity modulates long-term novelty response dynamics.

A. Ripple sequences were presented in blocks of entire REG or RND contexts. The novel ripple is always the same, allowing for potential adaptation to the novel ripple itself. **B, E.** Novelty responses over successive novel stimulus presentations, for example cells exhibiting adaptation (B) and facilitation (E) in neuronal responses to the novel ripple sequence in a REG context. Dots denote response strength for a individual novel ripple presentation and the dashed line is the best exponential fit. **C, F.** Exponential fits for adaptation (C) and facilitation (F) in REG (cyan) and RND (magenta) contexts across the population. **D, G.** Mean time constants for adaptation (D) and

facilitation (G) in REG and RND contexts for all neurons that exhibit such long-term dynamics. Both adaptation and facilitation are faster in the REG context (lower time constant, 2-way ANOVA, p = 0.0044).

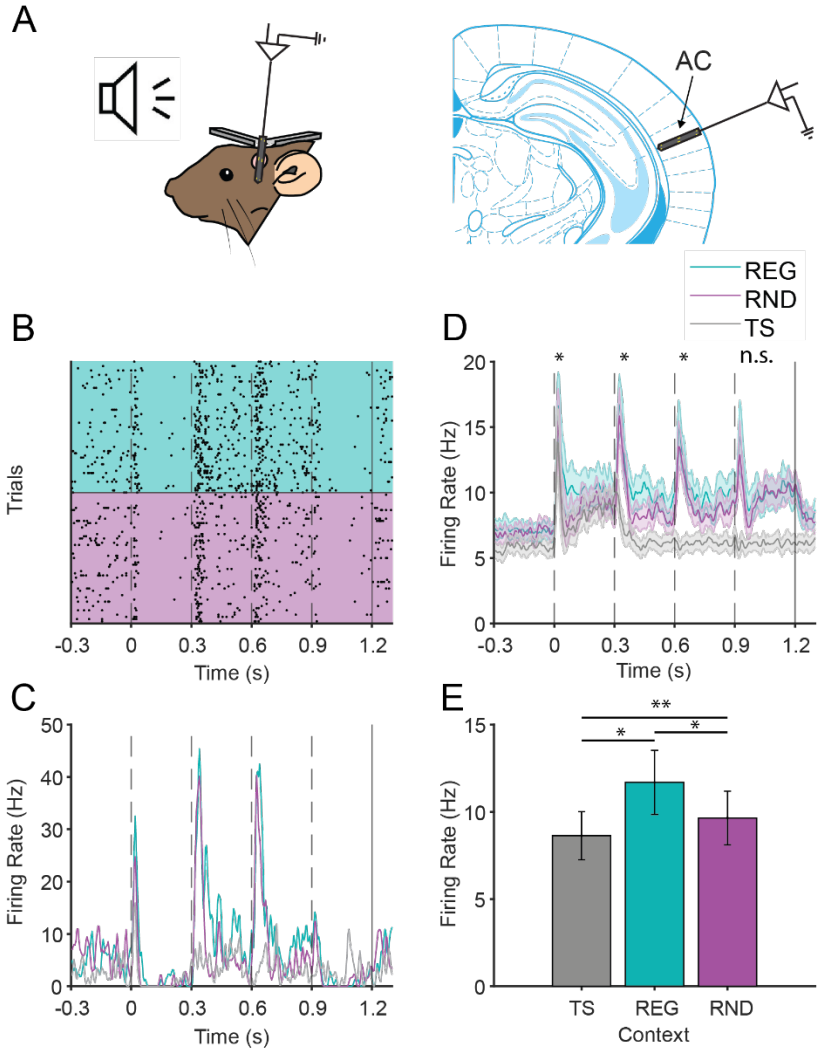

Figure 4

AC neurons exhibit higher firing rates to novel ripples in regular as compared to random contexts.

A. Left: schematic of electrophysiological recordings from AC in awake head-fixed mice. Right: Electrode superimposed on the AC outline from the Paxinos Brain Atlas (Paxinos and Franklin, 2012). **B.** Raster plot of spike times from an example neuron in response to the novel ripple sequence in REG (cyan) and RND (magenta) context. **C.** PSTH of the same neuron's firing rate in response to the novel ripple sequence in REG and RND as well as the tuning response to the first ripple in the novel sequence (grey). **D.** Mean firing rates over all neurons with a significant novelty response (n = 164) to the novel ripple sequence in REG (cyan), RND (magenta), and to the first ripple in isolation (grey). **E.** Mean firing rates in the first 100 ms post stimulus onset in REG, RND, and tuning contexts show a significant effect of context on novel ripple responses (repeated measures ANOVA, f(2) = 9.36, p = 0.00011). Error bars represent SEM.

Cortical neurons exhibit differential spiking responses to novel ripples in regular and random contexts

To resolve finer temporal information in cortical responses, we next performed electrophysiological recordings in the auditory cortex of awake mice (n = 5) while presenting the ripple stimuli (Figure 4A-C). From these recordings, we identified novelty responsive units using a paired t-test between the spike rates from the 300 ms following stimulus onset when the ripple was presented in isolation versus as a deviant and found that most neurons exhibited a novelty response in either context (55%, n = 164 neurons). Among the units with a significant novelty response, 59% responded with an increase in firing rate (n = 96 neurons). When comparing the firing rates in response to the novel ripple in the REG and RND contexts, there was a significant effect of context in the first 100 ms of the response (Figure 4D, E, repeated measures ANOVA, $f(2) = 9.36$, $p = 0.00011$). Novelty responses in the REG context were significantly greater than those in the RND context (post-hoc Tukey-Kramer, $p = 0.024$). Furthermore, the differential effect of context extended to the first 100 ms of the second (paired t-test, $p = 0.017$) and third (paired t-test, $p = 0.019$) ripples in the novel sequence but not the fourth (paired t-test, $p = 0.093$). When examining the last 100 ms of the response to the first ripple, although the mean firing rate was higher in the REG context (~10.2 Hz) compared to the RND context (~9.2 Hz), there was no significant effect of context (repeated measures ANOVA, $f(2) = 2.022$, $p = 0.13$). These results indicate that the information about context is integrated early in the responses of neurons in AC and support our findings from 2-photon imaging.

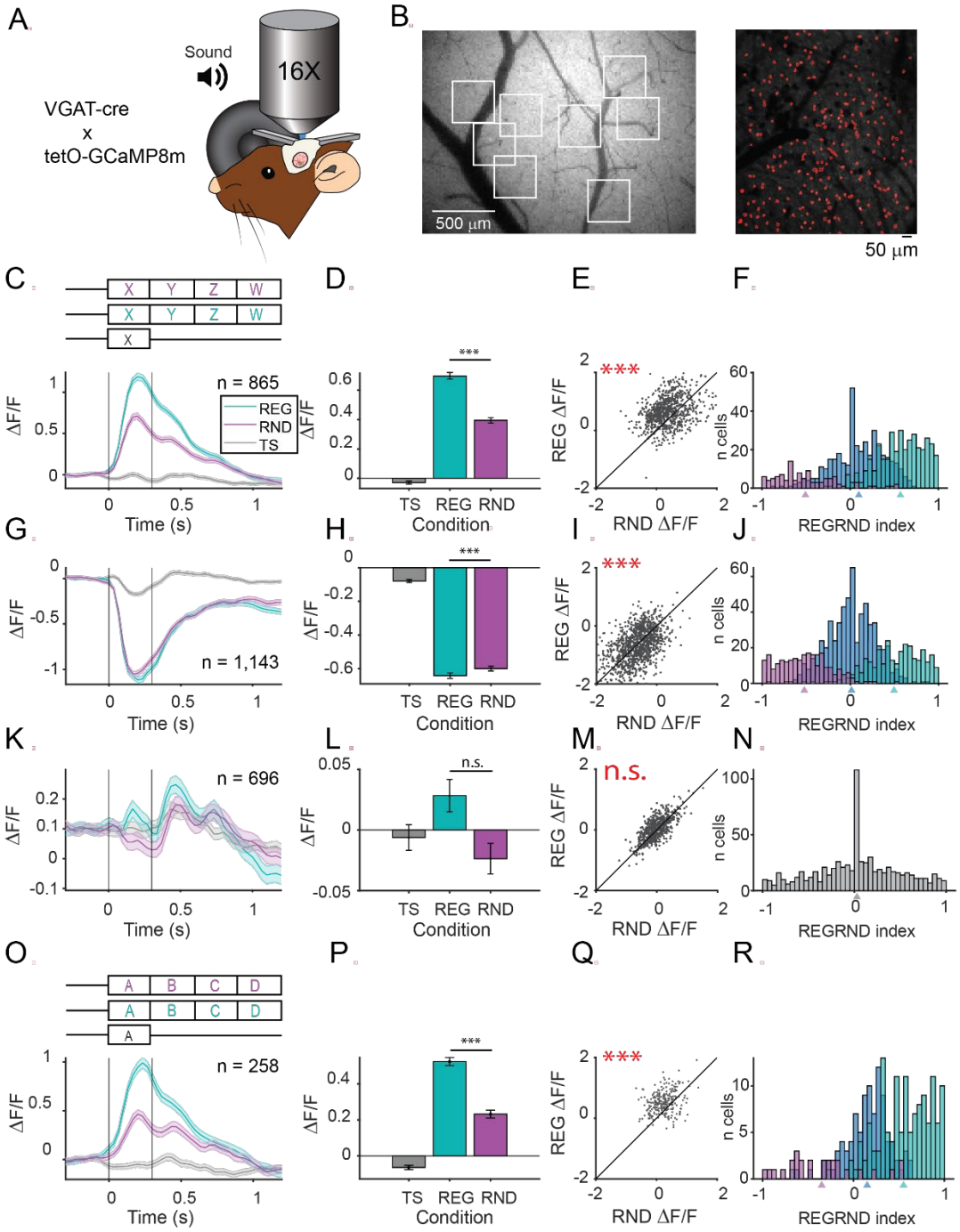

Figure 5

Inhibitory neurons in AC exhibit context-dependent novelty responses.

A. Schematic of 2-photon imaging from a transgenic mouse line expressing GCaMP8m only in inhibitory neurons. **B.** Left: Representative fields of view imaged (white boxes) overlayed on AC. For clarity, imaging areas close to one another have been combined. Right: representative field of view with identified neurons outlines using Suite2p. **C, G, K, O.** Population-averaged calcium traces across neurons with positive novelty response to the novel ripple presented in the REG

context (cyan), RND context (magenta), and as part of tuning stimulus (TS, grey) as z-scored ΔF/F on the left. Vertical lines represent duration of the first novel ripple. **D, H, L, P.** Mean responses to the novel ripple over 300 ms post stimulus onset in REG, RND and TS contexts. **E, I, M, Q.** Scatter plot of responses to the novel ripple under REG and RND contexts. **F, J, N, R.** Histogram of the REGRND index for responses to the novel ripple for neurons with preference for REG context (cyan), RND context (magenta) or no preferences (gray). Mean values for the index for each group are denoted by triangles below the x-axis. **C, D, E, F.** Responses to the novel ripple over neurons with positive novelty responses (n = 865, repeated measures ANOVA, p = 5.64e-26). REG novelty responses are significantly greater than RND novelty responses (post-hoc Tukey-Kramer, p = 3.83e-05). **G, H, I, J.** Similar to C-F, but for all negative novelty responses (n = 1,143, repeated measures ANOVA, p = 2.59e-42). For negative responses, REG novelty responses were significantly lower than RND responses (post-hoc Tukey-Kramer, p = 1.85e-06). **K, L, M, N.** Similar to C-F, but for average responses of all neurons without a significant novelty response (n 696, ANOVA, p = 0.98). There is no significant different between responses in REG and RND contexts. **O, P, Q, R.** Similar to C-F, but for recordings to stimuli in which background and novel ripples were swapped (ABCD was the novelty sequence and XYZW was the background sequence). (n = 258, repeated measures ANOVA, p < 4.62e-44). Responses in REG context are the strongest, followed by responses in RND context, followed by TS responses (post-hoc Tukey-Kramer, p = 1.19e-07).

Cortical inhibitory neurons exhibit contextually modulated novelty responses

Inhibitory neurons modulate novelty responses in AC (Natan et al., 2015; Yarden et al., 2022) as well as other sensory areas (Millman et al., 2020; Furutachi et al., 2024). In AC, cortical inhibitory neurons also exhibit the enhanced deviance response associated with SSA (Natan et al., 2015). We investigated whether cortical inhibitory neurons exhibit a similar novelty response to our ripple stimulus by imaging from a VGAT-Cre mouse line crossed with a transgenic Cre-dependent GCaMP8m line. This crossed line results in GCaMP8m expression only in inhibitory neurons. We found that, similar to our results from our pan-neuronal recordings, inhibitory neurons also exhibit a context-modulated novelty response (Figure 5). We found that 74.3% of cortical inhibitory neurons exhibited a significant novelty response. The REG context enhanced the response compared to the RND context for positive responses (72.2%, post-hoc Tukey-Kramer, p = 3.83e-05, Figure 5C-E), and negative responses in the REG context were stronger than in the RND (post-hoc Tukey-Kramer, p = 1.85e-06, Figure 5G-I). In a subset of recording sessions, we

presented a control stimulus sequence where the ripples used (ABCD or XYZW) for the background and novel sequences were swapped. Neurons from these sessions also exhibited an enhanced novelty response in the REG context compared to the RND context (post-hoc Tukey-Kramer, p = 1.19e-07, Figure 5O-Q). The REGRND index from the inhibitory neurons followed a similar pattern to our results from the general neuronal recordings. For positive responses, there is a significant preference for the REG context in neurons responsive to both contexts in the original (mean = 0.098, t-test, p = 1.31e-10, Figure 5F) and control sequences (mean = 0.154, t-test, p =7.02e-9, Figure 5R), while no significant effect was observed for negative responses (mean = 0.012, t-test, p = 0.25, Figure 5J). Furthermore, in contrast to the general population of neurons, the inhibitory neuronal population that did not exhibit a significant novelty response did not show a strong suppressive sound response (Figure 5K-N). The larger fraction of context-sensitive inhibitory neurons and larger context-evoked differences in the novelty responses in inhibitory neurons indicate that the novelty response found in the general population may be controlled by inhibitory neurons.

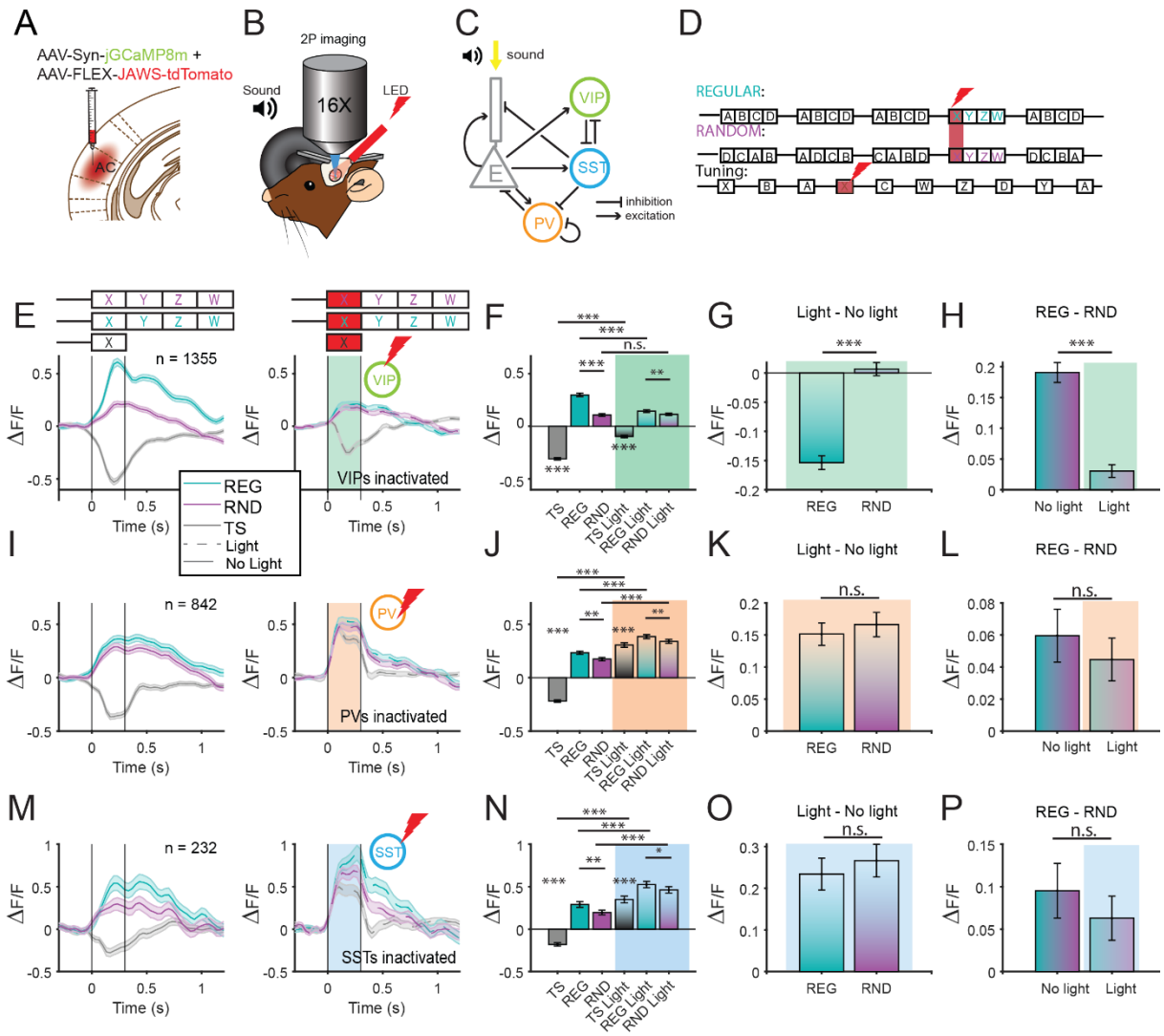

FIGURE 6

Selective context-dependent modulation of novelty responses by VIP neurons.

A, B, C, D. Schematics of the experimental set-up. **A.** Viral injection targeted to A1 included injection of a virus encoding GCaMP and a virus encoding a JAW-tdTomato construct in a Cre-dependent fashion into VIP-Cre, PV-Cre, or SST-Cre mice. Image from the Paxinos Brain atlas (Paxinos and Franklin, 2012). **B.** 2P imaging was performed in mice injected with JAWS-tdTomato in addition to GCaMP. **C.** Simplified diagram of the inhibitory-excitatory microcircuit in A1 that includes PV, SST and VIP neurons. PV neurons largely target the excitatory neuronal cell bodies, SST neurons target distal dendrites, whereas the VIP neurons inhibit SST neurons. **D.** Diagram of the stimulus with the light delivered during the novel stimulus presentation on a subset of trials. Optogenetic inactivation was performed during the first ripple in the novel sequence. **E, I, M.** Population-averaged calcium traces across neurons with positive novelty responses to the novel ripple presented in the REG context (cyan), RND context (magenta), and as part of tuning stimulus (grey) as z-scored ΔF/F. Left: light off; Right: light on. Vertical lines represent duration of the first novel ripple. **F, J, N.** Mean responses to novel ripple over 300 ms post stimulus onset in REG,

RND and TS contexts. Left: light off. Right: Light on. **G, K, O.** Mean changes in novelty responses due to inactivation of inhibitory neurons under REG (cyan) and RND (magenta) contexts. **H, L, P.** Mean difference in novelty responses between REG and RND contexts without light (left) and with light (during inhibitory neuron inactivation, right). **E, F, G, H.** Effects of inactivation of VIP inhibitory neurons. Inactivation of VIP neurons reduces the novelty response (n = 1,355, 2-way repeated measures ANOVA, p = 6.32e-20). This modulation of the novelty response is context-specific, with a much larger reduction in novelty responses under REG as compared to RND context (2-way repeated measures ANOVA, p = 2.24e-21). **I, J, K, L.** Effects of inactivation of PV inhibitory neurons. Inactivation of PV neurons increases the novelty response (n = 842, 2-way repeated measures ANOVA, p = 3.67e-22) and does not result in a differential effect of context (2-way repeated measures ANOVA, p = 0.40). **M, N, O, P.** Effects of inactivation of SST inhibitory neurons. Optogenetic inactivation of SST cells also increases the novelty response (n = 232, 2-way repeated measures ANOVA, p = 9.26e-12) but does not result in a differential effect of context (2-way repeated measures ANOVA, p = 0. 35).

Optogenetic inactivation of inhibitory neurons differentially modulates novelty responses

We next asked how specific classes of inhibitory neurons modulate cortical novelty detection in different contexts. Previous work has shown that PV and SST neurons differentially modulate stimulus-specific and temporal adaptation in AC (Natan et al., 2015, 2017). VIP neurons form a disinhibitory circuit with SST neurons and have also been shown to modulate novelty responses in sensory cortex (Furutachi et al., 2024). Therefore, we hypothesized that these distinct inhibitory neuron classes differentially modulate novelty responses in regular and random contexts. To investigate the role of inhibitory neurons in modulating the novelty response, we measured calcium activity in AC neurons while inactivating PV, SST, or VIP neurons using optogenetic activation of Jaws on a subset of trials (Figure 6A-D). Jaws is a red-shifted inhibitory opsin which we expressed selectively in each of three interneuron subtypes using Cre-expressing transgenic mice. We inactivated each of the three inhibitory neuron classes during the presentation of the first ripple in the novel sequence to identify their selective role in modulating the response. As expected, inactivating VIP neurons decreased response amplitude to ripples, whereas

558 inactivating SST or PV neurons increased the responses to ripples (Figure 6E-P, gray solid and
559 dashed lines).

560 For neurons with a positive novelty response, inactivation of VIP neurons decreased the
561 amplitude of the tuning response to the ripples (paired t-test, $p < 1e-20$, Figure 6E, F). The effect
562 of VIP neurons on novelty responses was selective for the temporal context (2-way repeated
563 measures ANOVA, p (Context x Light) = 2.24e-21, Figure 6E-H): suppressing VIP neurons
564 significantly reduced the novelty response in the regular (post-hoc Tukey-Kramer, $p < 1e-20$), but
565 not random contexts (post-hoc Tukey-Kramer, $p = 0.55$, Figure 6F, G). Furthermore, VIP
566 inactivation reduced the context-dependent difference in novelty responses (post-hoc Tukey-
567 Kramer, $p = 0.0032$, Figure 6H). Inactivating PV or SST neurons increased tuning responses to
568 the ripple, changing the mean response from negative to positive (paired t-test, $p_{PV} < 1e-20$, p_{SST}
569 $< 4.19e-29$, Figure 6I, J, M, N). Inactivating PV or SST neurons increased the novelty response
570 for both REG (post-hoc Tukey-Kramer, $p_{PV} < 1e-20$, Figure 6I-L, $p_{SST} < 1e-20$, Figure 6M-P) and
571 RND (post-hoc Tukey-Kramer, $p_{PV} < 1e-20$, Figure 6I-L, $p_{SST} < 1e-20$, Figure 6M-P) contexts.
572 However, there was no difference in the increase in novelty response due to the temporal context
573 (2-way repeated measures ANOVA, p_{PV} (Context x Light) = 0.40, Figure 6K, L, p_{SST} (Context x
574 Light) = 0.35, Figure 6O, P). Thus, VIP neurons selectively control the novelty responses in REG,
575 but not RND context, whereas PV and SST neurons reduce novelty responses in a context-
576 independent fashion.

577 For neurons that have negative novelty responses, optogenetic inactivation of all three
578 interneuron classes modulated the activity during the novel stimulus (Supplementary Figure 2).
579 For negative novelty responses, inactivating VIP neurons decreased the amplitude of novelty
580 responses under both random and regular contexts (2-way repeated measures ANOVA, $p < 1e-20$,

Supplementary Figure 2E-H). This modulation of novelty responses was context-dependent, with a stronger effect for regular as compared to random context (2-way repeated measures ANOVA, p(Context x Light) = 0. 015, Supplementary Figure 2G, H). Inactivating PV and SST neurons increased the novelty responses under both regular and random contexts (2-way repeated measures ANOVA, p_{PV} = 4.34e-41; p_{SST} = 3.41e-14, Supplementary Figure 2I-P). This change in novelty response was not context-dependent for either PV or SST neuron inactivation (PVs: 2-way repeated measures ANOVA, p = 0.53; SSTs: 2-way repeated measures ANOVA, p = 0.10, Supplementary Figure 2K, L, O, P). These results further support the differential function of VIP, but not SST or PV neurons under different contexts.

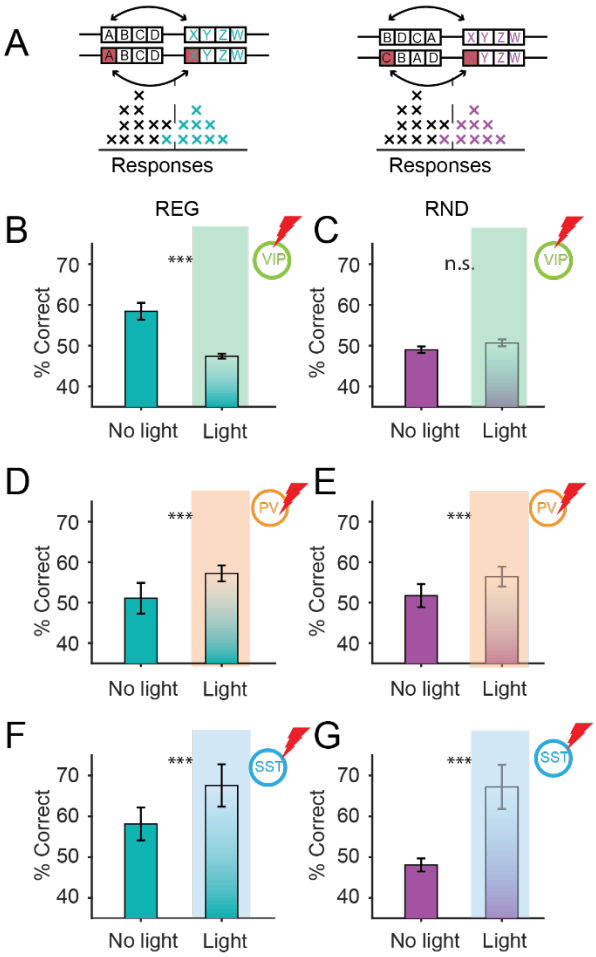

Figure 7

Differential effect of inhibitory neuronal inactivation on novelty detection under random and regular contexts.
A. Schematic of SVM classification for single neuronal responses to novel and context ripples. The activity during individual presentations of the context ripple and the novel ripple X was used to train the classifier under REG and RND contexts and during light and no light trials. **B-G.** Single neuron SVM performance for trials with (left) and without (right) light in the REG (B, D, F) and RND (C, E, G) contexts. **B, C.** VIP inactivation decreases SVM performance in REG context (post-hoc Tukey-Kramer, $p = 0.00036$), but not in RND context (post-hoc Tukey-Kramer, $p = 0.85$). **D, E.** PV inactivation improves SVM performance in REG context (post-hoc Tukey-Kramer, $p < 7.76e-7$) and in RND context (post-hoc Tukey-Kramer, $p = 0.00017$). **F, G.** SST inactivation improves SVM performance in REG context (post-hoc Tukey-Kramer, $p < 1.28e-7$) and in RND context (post-hoc Tukey-Kramer, $p < 4.98e-9$).

To understand how, across the positive and negative novelty responses, the inhibitory neurons affected novelty detection, we trained a support vector machine (SVM) classifier to differentiate between responses to a novel ripple and a context ripple (Figure 7A). For each recording session, we trained the classifier on the responses to the novel ripple X versus responses to the first ripple in the repeated background sequence. To match the position in the sequence as much as possible, we used the last repeat prior to the novel ripple on each trial. For regular contexts, this was always A, whereas for random contexts, this ripple varied between A, B, C and D. We compared the performance of the classifier in predicting whether neuronal responses corresponded to the novel or context ripple for trials with light (when the inhibitory neurons were suppressed) and without light, for the three different inhibitory neuron types.

We found that inactivating VIP neurons differentially modulated the classifier performance, reducing it only for the regular context condition, but not for the random context (post-hoc Tukey-Kramer, $p_{REG} < 0.00036$, post-hoc Tukey-Kramer, $p_{RND} < 0.85$, Figure 7B, C). In contrast, inactivating PV or SST neurons improved SVM performance under both random (post-hoc Tukey-Kramer, $p_{PV} < 0.00017$, post-hoc Tukey-Kramer, $p_{SST} < 4.98e-9$, Figure 7E, G) and regular (post-hoc Tukey-Kramer, $p_{PV} < 7.76e-7$, post-hoc Tukey-Kramer, $p_{SST} < 1.28e-7$, Figure

7D, F) contexts. These results are in line with the changes in the mean response strength that we observed (Figure 6). They furthermore suggest that the selective effects of inactivating VIP neurons for REG context persist for the discriminability of novel stimuli, whereas PV and SST neurons affect novelty responses, but not in a context-independent fashion.

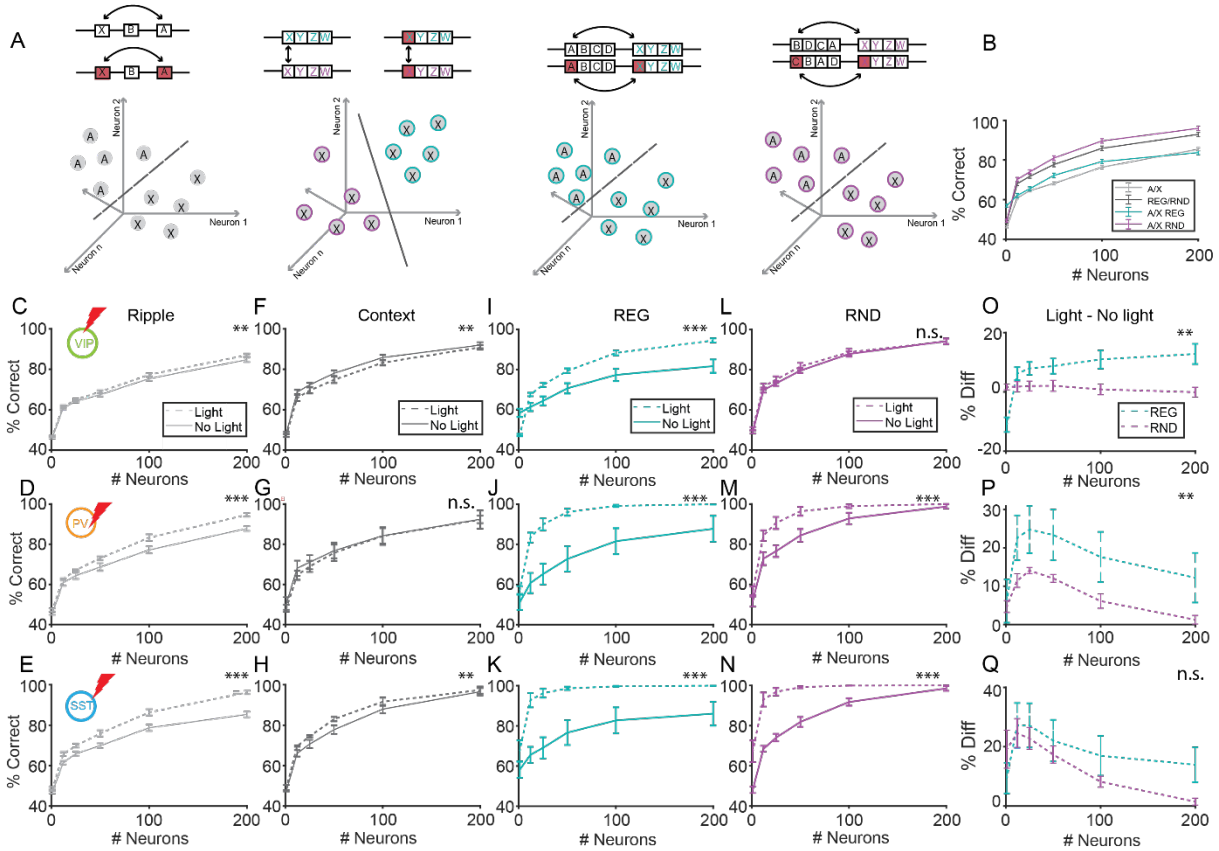

Figure 8.
Novelty decoding is improved with inhibitory neuron inactivation at the population level.
A. Schematic of a SVM identifying a linear decision boundary between points in a high dimensional space. We computed the SVM to discriminate between ripples A and X from the tuning response stimulus; for the novel ripple X under REG and RND contexts; for the novel ripple X versus background context ripple under REG; and RND contexts. All SVMs were trained and tested on data with and without optogenetic inactivation for each of the three inhibitory neuronal classes. **B.** SVM discrimination performance between context ripple and novel ripple X from the sound response stimulus (grey); discrimination performance of the novel ripple X between REG and RND contexts using the novelty response (black); novelty detection of X under REG (cyan) and RND (magenta) contexts. Context is easier to classify than ripple identity (2-way ANOVA, f(1)=196.25, p=9.38e-33). **C, D, E.** Effect of optogenetic inactivation of VIP (C), PV (D), and SST (E) neurons on ripple discrimination. Here and below, lines represent classifier performance; solid:

trials without light; dashed: trials with light. Inactivation of VIP (2-way ANOVA, f(1) = 7.45, p = 0.0072), PV (2-way ANOVA, f(1) = 27.50, p = 5.094e-6), and SST (2-way ANOVA, f(1) = 58.62, p = 1.98e-9) neurons all improved ripple discrimination performance. **F, G, H.** Effects of inactivation of VIP (F), PV (G), and SST (H) neurons on discrimination of novel ripple X under REG versus RND contexts. VIP inactivation decreased classification performance (2-way ANOVA, f(1) = 10.058, p = 0.0019) while SST inactivation improved performance (2-way ANOVA, f(1) = 12.47, p = 0.001), and PV inactivation did not have a significant effect (2-way ANOVA, f(1) = 0.67, p = 0.42). **I, J, K.** Effects of inactivation of VIP (I), PV (J), and SST (K) neurons on discriminating background and novel ripples under the REG context. All inactivations improved performance: PV (2-way ANOVA, f(1) = 50.18, p = 1.26e-8); SST (2-way ANOVA, f(1) = 58.45, p = 2.05e-9); VIP (2-way ANOVA, f(1) = 20.54, p = 1.26e-5) neuronal inactivation. **L, M, N.** Effects of inactivation of VIP (L), PV (M), and SST (N) neurons on discriminating background and novel ripples in the RND context. Both PV (2-way ANOVA, f(1) = 29.35, p = 2.91e-6) and SST neuronal inactivation (2-way ANOVA, f(1) = 75.31, p = 7.93e-9) enhanced performance, while VIP neuronal inactivation had no effect on classification performance (2-way ANOVA, f(1) = 3.02, p = 0.085). **O, P, Q.** Difference between classification performance with and without light inactivation for corresponding panels I-N. VIP inactivation (2-way ANOVA, f(1) = 9.8941, p = 0.0020) and PV inactivation (2-way ANOVA, f(1) = 14.407, p = 0. 0048) had significant differences in their effects on SVM discrimination performance across REG and RND contexts while SST inactivation did not (2-way ANOVA, f(1) = 1.5055, p = 0.23).

We next asked more broadly how these changes in novelty detection are implemented across the population of AC neurons. We expanded the discriminability analysis to multiple discrimination schemes and used subsets of progressively increasing numbers of neurons to train the SVMs. We found that discriminability increased with the number of neurons in the analysis and did not saturate at 200 neurons for any discrimination scheme (Figure 8A, B).

First, to establish a baseline in ripple discriminability based on the tuning stimulus, we computed the effect of inactivation of inhibitory neurons on discriminability between two ripples (Figure 8A left). PV and SST inactivation led to an increase in ripple discriminability, reaching higher than 90% discriminability at n = 200 neuron population size (2-way ANOVA, f(1) = 27.50, p_{PV} = 5.094e-6, Figure 8D; 2-way ANOVA, f(1) = 58.62, p_{SST} = 1.98e-9, Figure 8E). VIP inactivation had a significant, but much weaker effect (2-way ANOVA, f(1) = 7.45, p = 0.0072, Figure 8C, D, E). These results are consistent with prior studies that found that PV and SST neurons

affect neuronal tuning properties (Aizenberg et al., 2015; Li et al., 2015; Natan et al., 2015, 2017; Phillips and Hasenstaub, 2016; Kato et al., 2017; Phillips et al., 2017), whereas VIP neurons have an inconsistent effect on tuning in AC (Mesik et al., 2015; Tobin et al., 2024).

Next, we compared the SVM performance in discriminating the novelty response under REG versus RND contexts. If VIP neurons play a selective role in providing context-dependent information, we expected that their inactivation would impair the discriminability of novelty responses across REG and RND contexts. By contrast, for PV and SST neurons, we expected that their inactivation would have little effect on context discriminability. Indeed, we found that inactivating VIP neurons impaired context discriminability of novelty responses, which is consistent with a decrease in the difference in novelty responses under the two contexts (2-way ANOVA, $f(1) = 10.058$, $p = 0.0019$, Figure 8F). PV inactivation did not have a significant effect on context discriminability (Figure 8G), whereas SST inactivation improved the discriminability performance (2-way ANOVA, $f(1) = 12.47$, $p = 0.001$, Figure 8H).

Finally, we asked whether novelty detection under the two contexts improved with inhibitory neuronal inactivation. Surprisingly, we found that at a population level, inactivating all inhibitory neuron classes -- VIP, PV and SST neurons -- improved novelty detectability in REG context (2-way ANOVA, $f(1) = 20.54$, $p_{VIP} < 1.26e\text{-}5$, 2-way ANOVA, $f(1) = 50.18$, $p_{PV} < 1.26e\text{-}8$, 2-way ANOVA, $f(1)=58.45$, $p_{SST} < 2.05e\text{-}9$, Figure 8I, J, K). In RND context, VIP inactivation did not have an effect, whereas PV or SST inactivation also drove an improvement in novelty detection (2-way ANOVA, $f(1) = 29.35$, $p_{PV} < 2.90e\text{-}6$, 2-way ANOVA, $f(1) = 75.31$, $p_{SST} < 7.92e\text{-}11$, Figure 8 L, M, N). The effect PV or SST inactivation was strongest around a population of $n = 10\text{-}25$ neurons (Figure 8P, Q), suggesting that just a relatively small number of neurons can be involved in novelty detection. By contrast, the effect of VIP inactivation on novelty detection in

695 REG context increased with increasing number of neurons (Figure 8O), suggesting that VIP
696 neurons transmit the information about context to larger cortical populations. The finding that
697 novelty detection at population level is increased when any of the three inhibitory neuron types
698 are inactivated suggest that the cortical circuits operate in suboptimal regime in everyday hearing,
699 potentially allowing for context-dependent modulation by different inhibitory neuronal classes
700 (Tobin et al., 2024). This modulation is specific to regular context only for VIP neurons, in line in
701 our analysis of their differential effect on single neuronal responses (Figure 6).
702

703 **DISCUSSION**

704 In this study, we investigated how statistical regularity in sound sequences influences
705 cortical responses to novel auditory stimuli, and how inhibitory neurons contribute to this process.
706 Using calcium imaging and optogenetic inactivation in awake mice, we found that auditory cortex
707 (AC) neurons exhibited stronger novelty responses when novel sounds followed a regular context
708 compared to a random one. This enhancement was not uniform across cell types: while PV and
709 SST interneuron inactivation broadly increased novelty responses with mixed effect of context,
710 inactivation of VIP neurons selectively reduced novelty responses in the regular context. These
711 findings reveal a distinct role for VIP neurons in modulating context-dependent novelty detection
712 in AC.

713 Our results align with human studies showing that novelty detection is enhanced by
714 temporal predictability in sound streams. Previous EEG and behavioral work demonstrated that
715 listeners respond more robustly to violations in regular versus random sequences, but the
716 underlying neural circuitry was unknown (Barascud et al., 2016; Sohoglu and Chait, 2016;

717 Southwell and Chait, 2018). Here, by probing neuronal subtypes in mouse AC, we provide direct
718 evidence for circuit-level modulation of novelty responses by context. Our results suggest that
719 temporal regularity enhances novelty detection not merely by boosting adaptation or prediction
720 error in individual neurons (Ulanovsky et al., 2003, 2004; Natan et al., 2015, 2017; Parras et al.,
721 2017), but through targeted engagement of specific inhibitory networks.

722 A key contribution of this work is identifying VIP neurons as selective modulators of
723 context-dependent novelty responses. While VIP neurons have been implicated in disinhibitory
724 circuits across sensory cortical regions (Mesik et al., 2015; Pakan et al., 2016; Kuchibhotla et al.,
725 2017; Cone et al., 2019; Millman et al., 2020; Myers-Joseph et al., 2024; Tobin et al., 2024) and
726 have been implicated in oddball stimulus responses (Yarden et al., 2022), their role in encoding
727 statistical structure in naturalistic auditory stimuli was previously untested. We show that VIP
728 inactivation abolished the enhancement of novelty responses in the regular context without
729 affecting responses in the random context. This selective effect suggests that VIP neurons integrate
730 contextual information—potentially from top-down projections (Askew et al., 2019; Apicella and
731 Marchionni, 2022; Ferguson et al., 2023) — to gate prediction error signaling (Friston and Kiebel,
732 2009; Friston, 2010; Heilbron and Chait, 2018). In contrast, PV and SST neurons modulate gain
733 and adaptation more uniformly, regardless of context, consistent with their established roles in
734 first-order sensory processing.

735 Our findings also have implications for how auditory scenes are represented at the
736 population level. Using SVM-based decoding, we found that context information was more easily
737 extracted from single-neuron responses in the regular condition, while population-level decoding
738 performance plateaued more quickly. This shift toward a distributed, redundant code in regular

739 contexts may reflect a network reorganization mediated by VIP neurons, as previously shown in
740 auditory cortex (Tobin et al., 2024). Interestingly, inactivation of all interneuron types improved
741 decoding of novel stimulus identity, suggesting that inhibition refines but also constrains the
742 dynamic range of population responses.

743 One strength of our approach is the use of spectrally rich ripple stimuli, which elicit reliable
744 responses in a broad population of AC neurons. These stimuli better approximate the complexity
745 of natural sounds than pure tones and may engage higher-order auditory computations relevant to
746 speech, communication, and environmental navigation. Our observation that deviance detection
747 operates robustly across both excitatory and inhibitory populations reinforces the idea that
748 prediction-related computations are a core function of auditory cortex.

749 This work also opens new questions about the origins of context signals that modulate VIP
750 activity. VIP neurons are known to receive input from neuromodulatory and associative cortical
751 areas, including prefrontal cortex (Kuchibhotla et al., 2017; Askew et al., 2019; Apicella and
752 Marchionni, 2022; Ferguson et al., 2023; Ramamurthy et al., 2023). The selectivity of VIP
753 modulation for regular contexts may arise from top-down prediction signals that are absent in
754 random sequences. Future studies using pathway-specific manipulations or recordings in
755 interconnected regions will be needed to determine how these inputs shape VIP function (Furutachi
756 et al., 2024).

757 Several caveats warrant consideration. First, while we focused on layer 2/3 pyramidal
758 neurons, different interneuron subtypes span cortical layers and exhibit layer-specific functions.
759 Our widefield optogenetic inactivation likely affected VIP, PV, and SST neurons in multiple
760 layers, and the net effect observed in superficial recordings may reflect combined contributions

761 from distinct circuits (Meyer et al., 2011; Tremblay et al., 2016; Yavorska and Wehr, 2016; Naka
762 et al., 2019; Wu et al., 2022; David et al., 2023). Second, the precise nature of the statistical
763 computations—adaptation versus prediction error—encoded by each subtype remains to be
764 disentangled. Simultaneous recordings across AC layers and subcortical regions could further
765 clarify how prediction errors are computed and propagated.

766 In summary, our study demonstrates that statistical context modulates novelty detection in
767 auditory cortex through specific inhibitory circuits. We identify inhibitory neurons, and
768 specifically VIP neurons, as key players in shaping prediction-error signals based on contextual
769 statistical structure. These findings support models of predictive coding in sensory cortex and
770 suggest that context-sensitive disinhibition is a fundamental mechanism for flexible sensory
771 processing. By revealing how different inhibitory neurons contribute to novelty detection under
772 structured versus random auditory regimes, our results advance understanding of the neuronal
773 basis of auditory perception in complex environments.

774

775 **Table 1.**

Comparison	Figure	Test	N	Statistic	Effect Size	p-value
ANOVA for effects of REG/RND context on novelty response, all positive novelty responses	2b	One-way repeated measures ANOVA	2429	F(2)=1816.91	η2=0.428	<1e-20
Multiple comparison for REG, RND, and base sound response, all positive novelty responses	2c,d	post-hoc Tukey-Kramer	2429	MeanDifferenceBASEREG=-0.541 MeanDifferenceBASERND=-0.404 MeanDifferenceREGRND=0.136	n/a	5.96e-08 5.96e-08 5.96e-08
REGRND index for neurons responsive to both contexts, positive novelty	2e	t-test	769	Mean=0.0602	n/a	1.31e-10
ANOVA for effects of REG/RND context on novelty response, all negative novelty responses	2f	One-way repeated measures ANOVA	1962	F(2)=1324	η2=0.403	<1e-20
Multiple comparison for REG, RND, and base sound response, all negative novelty responses	2g,h	post-hoc Tukey-Kramer	1962	MeanDifferenceBASEREG=0.48 MeanDifferenceBASERND=0.464 MeanDifferenceREGRND=-0.0115	n/a	5.96e-08 5.96e-08 0.63
REGRND index for neurons responsive to both contexts, negative novelty	2i	t-test	634	Mean=0.0154	n/a	0.14
ANOVA for effects of REG/RND context on novelty response, all non-significant novelty responses	2j	One-way repeated measures ANOVA	4182	F(2)=3.8	η2=0.0009	0.023
Multiple comparison for REG, RND, and base sound response, all non-significant novelty responses	2k,l	post-hoc Tukey-Kramer	4182	MeanDifferenceBASEREG=-0.0075 MeanDifferenceBASERND=0.0053 MeanDifferenceREGRND=0.013	n/a	0.21 0.46 0.032
ANOVA for effects of REG/RND context on novelty response, positive novelty and sound response	2n	One-way repeated measures ANOVA	191	F(2)=129.72	η2=.4057	1.14e-43
Multiple comparison for REG, RND, and base sound response, positive novelty and sound response	2o,p	post-hoc Tukey-Kramer	191	MeanDifferenceBASEREG=-0.625 MeanDifferenceBASERND=-0.268 MeanDifferenceREGRND=0.358	n/a	5.96e-08 5.96e-08 5.96e-08
REGRND index for neurons responsive to both contexts, positive novelty and sound response	2q	t-test	51	Mean=12	n/a	0.0046
ANOVA for effects of REG/RND context and adaptation/facilitation on time constants	3d,g	Two-way ANOVA	8644	FREGRND(1)=8.1256 Fadaptfacil(1)=5.57e-6	η2=9.39e-4 η2=6.45e-10	0.0044 0.99
Difference in response to second novel ripple, first 100 ms	4d	paired t-test	164	MeanDifference=1.379	n/a	0.017
Difference in response to third novel ripple, first 100 ms	4d	paired t-test	164	MeanDifference=0.952	n/a	0.019

Difference in response to fourth novel ripple, first 100 ms	4d	paired t-test	164	MeanDifference=1.136	n/a	0.093
ANOVA for effect of context in novelty response for ephys	4e	repeated-measures anova	164	F(2)=9.3602	η2=0.0099598	0.00011
Multiple comparison for REG, RND, and base sound response, ephys	4e	post-hoc Tukey-Kramer	164	MeanDifferenceREGRND=0.0102 MeanDifferenceREGBASE=0.0153 MeanDifferenceRNDBASE=0.00507	n/a	0.024 0.0022 0.0091
ANOVA for effects of REG/RND context on novelty response, all positive novelty responses	5c	One-way repeated measures ANOVA	865	F(2)=79.10	η2=0.4441	5.64e-26
Multiple comparison for REG, RND, and base sound response, all positive novelty responses	5d,e	post-hoc Tukey-Kramer	865	MeanDifferenceBASEREG=-0.572 MeanDifferenceBASERND=-0.323 MeanDifferenceREGRND=0.249	n/a	1.19e-07 1.19e-07 3.83e-05
REGRND index for neurons responsive to both contexts, positive novelty	5f	t-test	865	Mean=0.0984	n/a	1.31e-10
ANOVA for effects of REG/RND context on novelty response, all negative novelty responses	5g	One-way repeated measures ANOVA	1143	F(2)=161.44	η2=0.6199	2.59e-42
Multiple comparison for REG, RND, and base sound response, all negative novelty responses	5h,i	post-hoc Tukey-Kramer	1143	MeanDifferenceBASEREG=0.72 MeanDifferenceBASERND=0.498 MeanDifferenceREGRND=-0.221	n/a	1.19e-07 1.19e-07 1.85e-06
REGRND index for neurons responsive to both contexts, negative novelty	5j	t-test	609	Mean=0.0124	n/a	0.25
ANOVA for effects of REG/RND context on novelty response, all non-significant novelty responses	5k	One-way repeated measures ANOVA	696	F(2)=0.02	η2=0.0002115	0.98
Multiple comparison for REG, RND, and base sound response, all non-significant novelty responses	5l,m	post-hoc Tukey-Kramer	696	MeanDifferenceBASEREG=-0.00199 MeanDifferenceBASERND=-0.00476 MeanDifferenceREGRND=-0.00277	n/a	0.99 0.98 0.99
ANOVA for effects of REG/RND context on novelty response, all positive novelty responses, swapped ripples	5o	One-way repeated measures ANOVA	258	F(2)=172.25	η2=0.635	4.62e-44
Multiple comparison for REG, RND, and base sound response, all positive novelty responses, swapped ripples	5p,q	post-hoc Tukey-Kramer	258	MeanDifferenceBASEREG=-0.631 MeanDifferenceBASERND=-0.295 MeanDifferenceREGRND=0.336	n/a	1.19e-07 1.19e-07 1.19e-07
REGRND index for neurons responsive to both contexts, positive novelty, swapped ripples	5r	t-test	258	Mean=0.154	n/a	7.02e-09
ANOVA for effects of context and optogenetic	6e,f,g,h	2-way repeated measures anova	1355	F(1)LIGHT=86.18 F(1)REGRND=104.19 F(1)Interaction=93.22	η2LIGHT=0.004937 η2REGRND=	6.32e-20 1.29e-23 2.24e-21

inactivation of VIPs on novelty responses					0.01119 η2Interaction= 0.005878	
Multiple comparison for REG, RND, and base sound response, VIP optogenetic inactivation	6f	post-hoc Tukey-Kramer	1355	MeanDifferenceRNDLIGHTNOLIGHT=-0.00669 MeanDifferenceREGLIGHTNOLIGHT=0.153 MeanDifferenceLIGHTREGRND=-0.0304 MeanDifferenceNOLIGHTREGRND=-0.191	n/a	0.55 <1e-20 0.0032 <1e-20
Baseline sound response, VIP inactivation	6f	t-test	1355	MeanNOLIGHT=-0.309 MeanLIGHT=-0.097	n/a	<1e-20 2.29e-17
Effect of inactivation of VIPs on baseline sound response	6f	paired t-test	1355	MeanDifference=-0.213	n/a	<1e-20
ANOVA for effects of context and optogenetic inactivation of PVs on novelty responses	6i,j,k,l	2-way repeated measures anova	842	F(1)LIGHT=99.18 F(1)REGRND=18.40 F(1)Interaction=0.72	η2LIGHT=0.01937 η2REGRND= 0.002087 η2Interaction= 4.25e-05	3.67e-22 2.00e-05 0.40
Multiple comparison for REG, RND, and base sound response, PV optogenetic inactivation	6j	post-hoc Tukey-Kramer	842	MeanDifferenceRNDLIGHTNOLIGHT=-0.166 MeanDifferenceREGLIGHTNOLIGHT=-0.151 MeanDifferenceLIGHTREGRND=-0.0447 MeanDifferenceNOLIGHTREGRND=-0.0595	n/a	<1e-20 <1e-20 0.00080 0.00030
Baseline sound response, PV inactivation	6j	t-test	842	MeanNOLIGHT=-0.219 MeanLIGHT=0.305	n/a	<1e-20 1.48e-42
Effect of inactivation of PVs on baseline sound response	6j	paired t-test	842	MeanDifference=-0.524	n/a	<1e-20
ANOVA for effects of context and optogenetic inactivation of SSTs on novelty responses	6m,n,o,p	2-way repeated measures anova	232	F(1)LIGHT=51.61 F(1)REGRND=11.21 F(1)Interaction=0.86	η2LIGHT=0.03647 η2REGRND= 0.003645 η2Interaction= 0.0001519	9.26e-12 0.00095 0.35
Multiple comparison for REG, RND, and base sound response, SST optogenetic inactivation	6n	post-hoc Tukey-Kramer	232	MeanDifferenceRNDLIGHTNOLIGHT=-0.266 MeanDifferenceREGLIGHTNOLIGHT=-0.234 MeanDifferenceLIGHTREGRND=-0.0629 MeanDifferenceNOLIGHTREGRND=-0.0952	n/a	<1e-20 <1e-20 0.016 0.0032
Baseline sound response, SST inactivation	6n	t-test	232	MeanNOLIGHT=-0.18 MeanLIGHT=0.349	n/a	9.27e-17 4.23e-16
Effect of inactivation of SSTs on baseline sound response	6n	paired t-test	232	MeanDifference=-0.529	n/a	4.19e-29
Multiple comparisons for SVM classification on REG background vs REG novel effects of light and population size with VIP inactivation	7b	post-hoc Tukey-Kramer	12	MeanDifference=-5.911	n/a	0.00036
Multiple comparisons for SVM classification on RND background	7c	post-hoc Tukey-Kramer	12	MeanDifference=-1.359	n/a	0.85

vs RND novel effects of light and population size with VIP inactivation						
Multiple comparisons for SVM classification on REG background vs REG novel effects of light and population size with PV inactivation	7d	post-hoc Tukey-Kramer	12	MeanDifference=-17.769	n/a	7.76e-07
Multiple comparisons for SVM classification on RND background vs RND novel effects of light and population size with PV inactivation	7e	post-hoc Tukey-Kramer	12	MeanDifference=-8.257	n/a	0.00017
Multiple comparisons for SVM classification on REG background vs REG novel effects of light and population size with SST inactivation	7f	post-hoc Tukey-Kramer	12	MeanDifference=-19.456	n/a	1.28e-07
Multiple comparisons for SVM classification on RND background vs RND novel effects of light and population size with SST inactivation	7g	post-hoc Tukey-Kramer	12	MeanDifference=-15.581	n/a	4.98e-9
ANOVA for SVM classification performance on context and ripple identity	8b	2-way anova	20	Fpopsize(5)=519.13 Fcontextripple(1)=196.25	η2=0.86 η2=0.065	4.12e-124 9.38e-33
ANOVA for SVM classification performance on background and novel in REG vs RND contexts	8b	2-way anova	20	Fpopsize(5)=106.91 Fregrnd1)=41.371	η2=0.66 η2=0.051	2.70e-58 7.070e-10
Multiple comparisons for SVM classification REG vs RND no light	8b	post-hoc Tukey-Kramer	20	MeanDifference=-6.7395	n/a	7.30e-09
ANOVA for SVM performance on ripple identity in VIP mice	8c	2-way anova	12	Fpopsize(5)=548.12 Flightnolight(1)=7.4468	η2=0.95 η2=0.0026	1.077e-88 0.0072
ANOVA for SVM performance on ripple identity in PV mice	8d	2-way anova	4	Fpopsize(5)=284.2 Flightnolight(1)=27.503	η2=0.95 η2=0.0185	1.11e-30 5.094e-06
ANOVA for SVM performance on ripple identity in SST mice	8e	2-way anova	4	Fpopsize(5)=261.82 Fclass(1)=58.62	η2=0.929 η2=0.0291	5.66-30 1.98e-09
ANOVA for SVM performance on context identity in VIP mice	8f	2-way anova	12	Fpopsize(5)=296.12 Fclass(1)=10.058	η2=0.910 η2=0.0062	1.39e-71 0.0019
ANOVA for SVM performance on context identity in PV mice	8g	2-way anova	4	Fpopsize(5)=42.809 Fclass(1)=0.67358	η2=0.837 η2=0.0026	3.17e-15 0.42
ANOVA for SVM performance on context identity in SST mice	8h	2-way anova	4	Fpopsize(5)=258.65 Fclass(1)=12.465	η2= 0.960 η2=0.0093	7.21e-30 0.0010

ANOVA for SVM performance on background vs novel in REG in VIP mice	8i	2-way anova	12	Fpopsize(5)= 64.1 Fclass(1)=20.543	η2=0.671 η2=0.0430	3.45e-34 1.26e-05
ANOVA for SVM performance on background vs novel in REG in PV mice	8j	2-way anova	4	Fpopsize(5)=22.11 Fclass(1)=50.178	η2=0.548 η2=0.249	1.12e-10 1.26e-08
ANOVA for SVM performance on background vs novel in REG in SST mice	8k	2-way anova	4	Fpopsize(5)=12.54 Fclass(1)=58.452	η2= 0.387 η2=0.361	2.056e-07 2.054e-09
ANOVA for SVM performance on background vs novel in RND in VIP mice	8l	2-way anova	12	Fpopsize(5)=265.13 Fclass(1)=3.016	η2=0.91 η2=0.0021	1.35e-68 0.085
ANOVA for SVM performance on background vs novel in RND in PV mice	8m	2-way anova	4	Fpopsize(5)=77.016 Fclass(1)=29.35	η2=0.85 η2=0.064	9.49e-20 2.90e-06
ANOVA for SVM performance on background vs novel in RND in SST mice	8n	2-way anova	4	Fpopsize(5)=46.278 Fclass(1)=75.309	η2= 0.67 η2=0.26	8.36e-16 7.92e-11
ANOVA for SVM performance difference on background vs novel in REG/RND in VIP mice	8o	2-way anova	24	Fpopsize(5)=5.5069 Fclass(1)=9.8941	η2=0.16 η2=0.057	0.00012 0.0020
ANOVA for SVM performance difference on background vs novel in REG/RND in PV mice	8p	2-way anova	8	Fpopsize(5)=3.7646 Fclass(1)=14.407	η2=0.25 η2=0.19	0.0068 0.00048
ANOVA for SVM performance difference on background vs novel in REG/RND in SST mice	8q	2-way anova	8	Fpopsize(5)= 3.4993 Fclass(1)= 1.5055	η2= 0.29 η2=0.025	0.010 0.23
ANOVA for effects of context and optogenetic inactivation of VIPs on negative novelty responses	s2e,f,g,h	2-way repeated measures anova	1062	F(1)LIGHT=493.60 F(1)REGRND=1.12 F(1)Interaction=5.94	η2LIGHT=0.02737 η2REGRND=0.000116 η2Interaction=0.00039	<1e-20 0.29 0.015
Multiple comparison for REG, RND, and base sound response, VIP optogenetic inactivation	s2f	post-hoc Tukey-Kramer	1062	MeanDifferenceRNDLIGHTNOLIGHT=-0.179 MeanDifferenceREGLIGHTNOLIGHT=-0.228 MeanDifferenceLIGHTREGRND=-0.0375 MeanDifferenceNOLIGHTREGRND=0.011	n/a	<1e-20 <1e-20 0.0024 0.56
Baseline sound response, VIP inactivation	s2f	t-test	1062	MeanNOLIGHT=0.0703 MeanLIGHT=-0.0146	n/a	1.9e-07 0.27
Effect of inactivation of VIPs on baseline sound response	s2f	paired t-test	1062	MeanDifference=-0.213	n/a	2.67e-13
ANOVA for effects of context and optogenetic inactivation of PVs on negative novelty responses	s2i,j,k,l	2-way repeated measures anova	662	F(1)LIGHT=207.36 F(1)REGRND=3.98 F(1)Interaction=0.40	η2LIGHT=0.058 η2REGRND=0.00050	4.34e-41 0.046 0.53

					η2Interaction= 2.078e-05	
Multiple comparison for REG, RND, and base sound response, PV optogenetic inactivation	s2j	post-hoc Tukey-Kramer	662	MeanDifferenceRNDLIGHTNOLIGHT=-0.305 MeanDifferenceREGLIGHTNOLIGHT=-0.293 MeanDifferenceLIGHTREGRND=-0.0221 MeanDifferenceNOLIGHTREGRND=-0.0334	n/a	<1e-20 <1e-20 0.12 0.072
Baseline sound response, PV inactivation	s2j	t-test	662	MeanNOLIGHT=0.0021 MeanLIGHT=0.25	n/a	0.87 7.42e-17
Effect of inactivation of PVs on baseline sound response	s2j	paired t-test	662	MeanDifference=-0.248	n/a	5.99e-17
ANOVA for effects of context and optogenetic inactivation of SSTs on negative novelty responses	s2m,n,o,p	2-way repeated measures anova	238	F(1)LIGHT=65.20 F(1)REGRND=63.46 F(1)Interaction=2.70	η2LIGHT=0.0603 η2REGRND=0.019 η2Interaction=0.00054	3.41e-14 6.84e-14 0.10
Multiple comparison for REG, RND, and base sound response, SST optogenetic inactivation	s2n	post-hoc Tukey-Kramer	238	MeanDifferenceRNDLIGHTNOLIGHT=-0.321 MeanDifferenceREGLIGHTNOLIGHT=-0.266 MeanDifferenceLIGHTREGRND=0.194 MeanDifferenceNOLIGHTREGRND=0.139	n/a	<1e-20 <1e-20 <1e-20 1.85e-06
Baseline sound response, SST inactivation	s2n	t-test	238	MeanNOLIGHT=-0.0917 MeanLIGHT=0.205	n/a	8.60e-07 1.22e-05
Effect of inactivation of SSTs on baseline sound response	s2n	paired t-test	238	MeanDifference=-0.113	n/a	0.011
Difference between sound response with and without light in all mice	s3b	paired t-test	8573	MeanDifference=-0.455	n/a	5.55e-139
Difference between sound response with and without light in control mice	s3d	paired t-test	284	MeanDifference=-0.0599	n/a	0.0151

Bibliography

Aizenberg M, Mwilambwe-Tshilobo L, Briguglio JJ, Natan RG, Geffen MN (2015) Bidirectional Regulation of Innate and Learned Behaviors That Rely on Frequency Discrimination by Cortical Inhibitory Neurons. PLoS Biology 13.

Antunes FM, Nelken I, Covey E, Malmierca MS (2010) Stimulus-specific adaptation in the auditory thalamus of the anesthetized rat. PloS one 5:e14071.

Apicella A junior, Marchionni I (2022) VIP-Expressing GABAergic Neurons: Disinhibitory vs. Inhibitory Motif and Its Role in Communication Across Neocortical Areas. Front Cell Neurosci 16 Available at: https://www.frontiersin.org/articles/10.3389/fncel.2022.811484 [Accessed April 26, 2024].

Arnal LH, Giraud A-L (2012) Cortical oscillations and sensory predictions. Trends in Cognitive Sciences 16:390–398.

Askew CE, Lopez AJ, Wood MA, Metherate R (2019) Nicotine excites VIP interneurons to disinhibit pyramidal neurons in auditory cortex. Synapse 73:e22116.

Attinger A, Wang B, Keller GB (2017) Visuomotor Coupling Shapes the Functional Development of Mouse Visual Cortex. Cell 169:1291-1302.e14.

Barascud N, Pearce MT, Griffiths TD, Friston KJ, Chait M (2016) Brain responses in humans reveal ideal observer-like sensitivity to complex acoustic patterns. Proceedings of the National Academy of Sciences 113:E616–E625.

Betzel RF, Wood KC, Angeloni C, Geffen MN, Bassett DS (2019) Stability of spontaneous, correlated activity in mouse auditory cortex. PLOS Computational Biology 15:e1007360.

Chen I-W, Helmchen F, Lütcke H (2015) Specific Early and Late Oddball-Evoked Responses in Excitatory and Inhibitory Neurons of Mouse Auditory Cortex. J Neurosci 35:12560–12573.

Chuong AS et al. (2014) Noninvasive optical inhibition with a red-shifted microbial rhodopsin. Nature neuroscience 17:1123.

Cone JJ, Scantlen MD, Histed MH, Maunsell JHR (2019) Different Inhibitory Interneuron Cell Classes Make Distinct Contributions to Visual Contrast Perception. eNeuro 6:ENEURO.0337-18.2019.

David F, Borel M, Ayub S, Ruther P, Gentet LJ (2023) Layer-specific stimulations of parvalbumin-positive cortical interneurons in mice entrain brain rhythms to different frequencies. Cereb Cortex 33:8286–8299.

Farley BJ, Quirk MC, Doherty JJ, Christian EP (2010) Stimulus-Specific Adaptation in Auditory Cortex Is an NMDA-Independent Process Distinct from the Sensory Novelty Encoded by the Mismatch Negativity. J Neurosci 30:16475–16484.

Ferguson KA, Salameh J, Alba C, Selwyn H, Barnes C, Lohani S, Cardin JA (2023) VIP interneurons regulate cortical size tuning and visual perception. Cell Rep 42:113088.

Friston K (2010) The free-energy principle: a unified brain theory? Nat Rev Neurosci 11:127–138.

Friston K, Kiebel S (2009) Predictive coding under the free-energy principle. Philosophical Transactions of the Royal Society B: Biological Sciences 364:1211–1221.

Furutachi S, Franklin AD, Aldea AM, Mrsic-Flogel TD, Hofer SB (2024) Cooperative thalamocortical circuit mechanism for sensory prediction errors. Nature 633:398–406.

Harms L, Fulham WR, Todd J, Budd TW, Hunter M, Meehan C, Penttonen M, Schall U, Zavitsanou K, Hodgson DM, Michie PT (2014) Mismatch Negativity (MMN) in Freely-Moving Rats with Several Experimental Controls. PLOS ONE 9:e110892.

Hattori R, Komiyama T (2022) PatchWarp: Corrections of non-uniform image distortions in two-photon calcium imaging data by patchwork affine transformations. Cell Reports Methods 2:100205.

Heilbron M, Chait M (2018) Great Expectations: Is there Evidence for Predictive Coding in Auditory Cortex? Neuroscience 389:54–73.

Hershenhoren I, Taaseh N, Antunes FM, Nelken I (2014) Intracellular correlates of stimulus-specific adaptation. The Journal of neuroscience : the official journal of the Society for Neuroscience 34:3303–3319.

Johnson KR, Tian C, Gagnon LH, Jiang H, Ding D, Salvi R (2017) Effects of Cdh23 single nucleotide substitutions on age-related hearing loss in C57BL/6 and 129S1/Sv mice and comparisons with congenic strains. Sci Rep 7:44450.

Kato HK, Asinof SK, Isaacson JS (2017) Network-Level Control of Frequency Tuning in Auditory Cortex. Neuron.

Kuchibhotla KV, Gill JV, Lindsay GW, Papadoyannis ES, Field RE, Sten TAH, Miller KD, Froemke RC (2017) Parallel processing by cortical inhibition enables context-dependent behavior. Nature neuroscience 20:62–71.

Lee S, Hjerling-Leffler J, Zagha E, Fishell G, Rudy B (2010) The Largest Group of Superficial Neocortical GABAergic Interneurons Expresses Ionotropic Serotonin Receptors. J Neurosci 30:16796–16808.

Lesicko AMH, Angeloni CF, Blackwell JM, De Biasi M, Geffen MN (2022) Corticofugal regulation of predictive coding. Elife 11:e73289.

Levy RB, Reyes AD (2012) Spatial Profile of Excitatory and Inhibitory Synaptic Connectivity in Mouse Primary Auditory Cortex. Journal of Neuroscience 32:5609–5619.

Li LY, Xiong XR, Ibrahim LA, Yuan W, Tao HW, Zhang LI (2015) Differential Receptive Field Properties of Parvalbumin and Somatostatin Inhibitory Neurons in Mouse Auditory Cortex. Cerebral cortex 25:1782–1791.

Malmierca MS, Anderson LA, Antunes FM (2015) The cortical modulation of stimulus-specific adaptation in the auditory midbrain and thalamus: a potential neuronal correlate for predictive coding. Front Syst Neurosci 9:19.

Mehra M, Mukesh A, Bandyopadhyay S (2022) Separate Functional Subnetworks of Excitatory Neurons Show Preference to Periodic and Random Sound Structures. J Neurosci 42:3165–3183.

Mesik L, Ma W, Li L, Ibrahim LA, Huang ZJ, Zhang LI, Tao HW (2015) Functional response properties of VIP-expressing inhibitory neurons in mouse visual and auditory cortex. Front Neural Circuits 9:22.

Meyer HS, Schwarz D, Wimmer VC, Schmitt AC, Kerr JND, Sakmann B, Helmstaedter M (2011) Inhibitory interneurons in a cortical column form hot zones of inhibition in layers 2 and 5A. Proceedings of the National Academy of Sciences 108:16807–16812.

Millman DJ, Ocker GK, Caldejon S, Kato I, Larkin JD, Lee EK, Luviano J, Nayan C, Nguyen TV, North K, Seid S, White C, Lecoq J, Reid C, Buice MA, de Vries SE (2020) VIP interneurons in mouse primary visual cortex selectively enhance responses to weak but specific stimuli Vinck M, Wassum KM, eds. eLife 9:e55130.

Myers-Joseph D, Wilmes KA, Fernandez-Otero M, Clopath C, Khan AG (2024) Disinhibition by VIP interneurons is orthogonal to cross-modal attentional modulation in primary visual cortex. Neuron 112:628-645.e7.

Naatanen R, Gaillard AW, Mantysalo S (1978) Early selective-attention effect on evoked potential reinterpreted. Acta psychologica 42:313–329.

Naatanen R, Paavilainen P, Rinne T, Alho K (2007) The mismatch negativity (MMN) in basic research of central auditory processing: a review. Clin Neurophysiol 118:2544–2590.

Naatanen R, Pakarinen S, Rinne T, Takegata R (2004) The mismatch negativity (MMN): towards the optimal paradigm. Clin Neurophysiol 115:140–144.

Naka A, Veit J, Shababo B, Chance RK, Risso D, Stafford D, Snyder B, Egladyous A, Chu D, Sridharan S, Mossing DP, Paninski L, Ngai J, Adesnik H (2019) Complementary networks of cortical somatostatin interneurons enforce layer specific control. Elife 8:e43696.

Natan RG, Briguglio JJ, Mwilambwe-Tshilobo L, Jones SI, Aizenberg M, Goldberg EM, Geffen MN (2015) Complementary control of sensory adaptation by two types of cortical interneurons. eLife 4:1–27.

Natan RG, Rao W, Geffen MN (2017) Cortical Interneurons Differentially Shape Frequency Tuning following Adaptation. Cell Reports 21:878–890.

Nelken I (2004) Processing of complex stimuli and natural scenes in the auditory cortex. Current opinion in neurobiology 14:474–480.

Nelken I (2014) Stimulus-specific adaptation and deviance detection in the auditory system: experiments and models. Biological cybernetics Available at: http://www.ncbi.nlm.nih.gov/pubmed/24477619.

Pachitariu M, Steinmetz N, Kadir S, Carandini M, D HK (2016) Kilosort: realtime spike-sorting for extracellular electrophysiology with hundreds of channels. :061481 Available at: https://www.biorxiv.org/content/10.1101/061481v1 [Accessed February 6, 2025].

Pachitariu M, Stringer C, Dipoppa M, Schröder S, Rossi LF, Dalgleish H, Carandini M, Harris KD (2017) Suite2p: beyond 10,000 neurons with standard two-photon microscopy. bioRxiv:061507.

Pakan JM, Lowe SC, Dylda E, Keemink SW, Currie SP, Coutts CA, Rochefort NL (2016) Behavioral-state modulation of inhibition is context-dependent and cell type specific in mouse visual cortex Mrsic-Flogel TD, ed. eLife 5:e14985.

Parras GG, Nieto-Diego J, Carbajal GV, Valdés-Baizabal C, Escera C, Malmierca MS (2017) Neurons along the auditory pathway exhibit a hierarchical organization of prediction error. Nat Commun 8:2148.

Paxinos G, Franklin KB (2012) The Mouse Brain in Stereotaxic Coordinates. Sydney: Academic Press.

Phillips EA, Hasenstaub AR (2016) Asymmetric effects of activating and inactivating cortical interneurons. eLife 5 Available at: https://www.ncbi.nlm.nih.gov/pubmed/27719761.

Phillips EAK, Schreiner CE, Hasenstaub AR (2017) Cortical Interneurons Differentially Regulate the Effects of Acoustic Context. Cell Rep 20:771–778.

Ramamurthy DL, Chen A, Zhou J, Park C, Huang PC, Bharghavan P, Krishna G, Liu J, Casale K, Feldman DE (2023) VIP interneurons in sensory cortex encode sensory and action signals but not direct reward signals. Current Biology 33:3398-3408.e7.

Rubin J, Ulanovsky N, Nelken I, Tishby N (2016) The Representation of Prediction Error in Auditory Cortex. PLoS Comput Biol 12:1005058.

Siegle JH, López AC, Patel YA, Abramov K, Ohayon S, Voigts J (2017) Open Ephys: an open-source, plugin-based platform for multichannel electrophysiology. J Neural Eng 14:045003.

Sohoglu E, Chait M (2016) Detecting and representing predictable structure during auditory scene analysis. eLife 5:1–17.

Solyga M, Keller GB (2025) Multimodal mismatch responses in mouse auditory cortex. eLife 13 Available at: https://elifesciences.org/reviewed-preprints/95398 [Accessed February 19, 2025].

Southwell R, Chait M (2018) Enhanced deviant responses in patterned relative to random sound sequences. Cortex 109:92–103.

Szymanski FD, Garcia-Lazaro JA, Schnupp JWH (2009) Current Source Density Profiles of Stimulus-Specific Adaptation in Rat Auditory Cortex. Journal of Neurophysiology 102:1483–1490.

Tobin M, Sheth J, Wood KC, Michel EK, Geffen MN (2024) Distinct inhibitory neurons differently shape neuronal codes for sound intensity in the auditory cortex. J Neurosci Available at: https://www.jneurosci.org/content/early/2024/11/06/JNEUROSCI.1502-23.2024 [Accessed December 16, 2024].

Tremblay R, Lee S, Rudy B (2016) GABAergic Interneurons in the Neocortex: From Cellular Properties to Circuits. Neuron 91:260–292.

Ulanovsky N, Las L, Farkas D, Nelken I (2004) Multiple time scales of adaptation in auditory cortex neurons. Journal of Neuroscience 24:10440–10453.

Ulanovsky N, Las L, Nelken I (2003) Processing of low-probability sounds by cortical neurons. Nature Neuroscience 6:391–398.

Vapnik V (2013) The Nature of Statistical Learning Theory. Springer Science & Business Media.

Vogler NW, Chen R, Virkler A, Tu VY, Gottfried JA, Geffen MN (2024) Direct Piriform-to-Auditory Cortical Projections Shape Auditory–Olfactory Integration. J Neurosci 44 Available at: https://www.jneurosci.org/content/44/49/e1140242024 [Accessed February 6, 2025].

Wood KC, Angeloni CF, Oxman K, Clopath C, Geffen MN (2022) Neuronal activity in sensory cortex predicts the specificity of learning in mice. Nature Communications 13.

Wood KC, Blackwell JM, Geffen MN (2017) Cortical inhibitory interneurons control sensory processing. Current Opinion in Neurobiology 46:200–207.

Wu J, Zhao Z, Shi Y, He M (2022) Cortical VIP+ Interneurons in the Upper and Deeper Layers Are Transcriptionally Distinct. J Mol Neurosci 72:1779–1795.

Yarden TS, Mizrahi A, Nelken I (2022) Context-Dependent Inhibitory Control of Stimulus-Specific Adaptation. J Neurosci 42:4629–4651.

Yaron A, Hershenhoren I, Nelken I (2012) Sensitivity to Complex Statistical Regularities in Rat Auditory Cortex. Neuron 76:603–615.

Yavorska I, Wehr MS (2016) Somatostatin-Expressing Inhibitory Interneurons in Cortical Circuits. Frontiers in Neural Circuits 10:1–18.

Figure 1

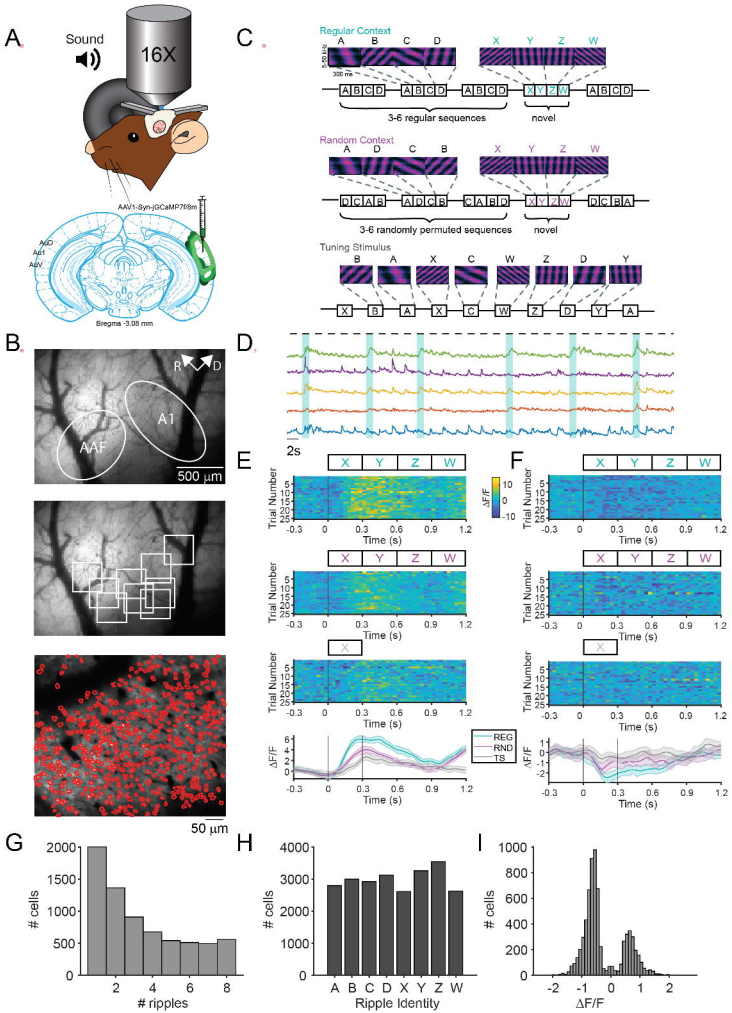
A
Sound
16X
AAV1-Syn-jGCaMP7f8m
AAD
Aal
AAV
Bregma -3.08 mm
B
R
D
AAF
A1
500 µm
50 µm
C
Regular Context
A B C D
X Y Z W
5.50 kHz
300 ms
ABCD ABCD ABCD XYZW ABCD
3-6 regular sequences
novel
Random Context
A D C B
X Y Z W
DCAB ADCB CABD XYZW DCBA
3-6 randomly permuted sequences
novel
Tuning Stimulus
B A X C W Z D Y
X B A X C W Z D Y A
D
E
2s
X Y Z W
Trial Number
Time (s)
ΔF/F
REG
RND
TS
F
G
cells
ripples
H
Ripple Identity
I
ΔF/F

Figure 2

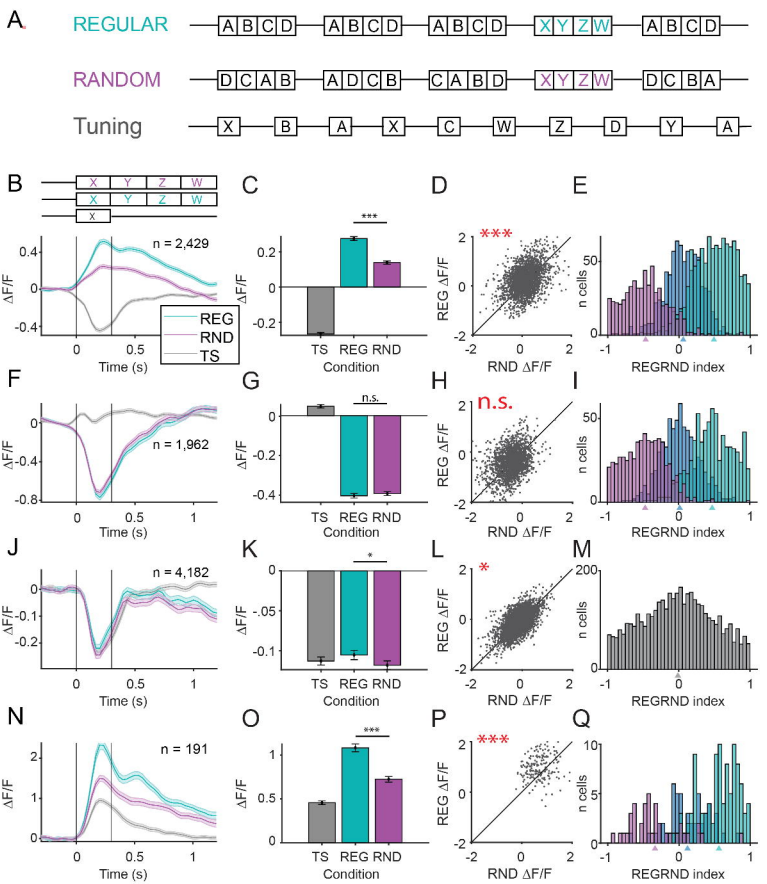
A
REGULAR
A B C D
A B C D
A B C D
X Y Z W
A B C D
RANDOM
D C A B
A D C B
C A B D
X Y Z W
D C B A
Tuning
X B A X C W Z D Y A
B
X Y Z W
X Y Z W
X
n = 2,429
ΔF/F
Time (s)
REG
RND
TS
C
***
ΔF/F
TS REG RND
Condition
D
***
REG ΔF/F
RND ΔF/F
E
n cells
REGRND index
F
n = 1,962
G
n.s.
H
n.s.
I
J
n = 4,182
K
*
L
*
M
N
n = 191
O
***
P
***
Q

Figure 3

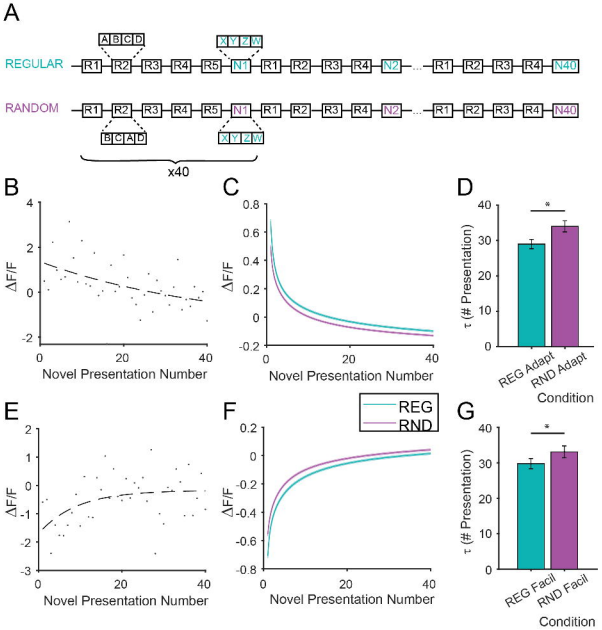
A
ABCD
XYZM
REGULAR
R1 R2 R3 R4 R5 N1 R1 R2 R3 R4 N2 ... R1 R2 R3 R4 N40
RANDOM
R1 R2 R3 R4 R5 N1 R1 R2 R3 R4 N2 ... R1 R2 R3 R4 N40
BCAD
XYZM
x40
B
ΔF/F
Novel Presentation Number
C
ΔF/F
Novel Presentation Number
D
τ (# Presentation)
*
REG Adapt
RND Adapt
Condition
E
ΔF/F
Novel Presentation Number
F
REG
RND
ΔF/F
Novel Presentation Number
G
τ (# Presentation)
*
REG Facil
RND Facil
Condition

Figure 4

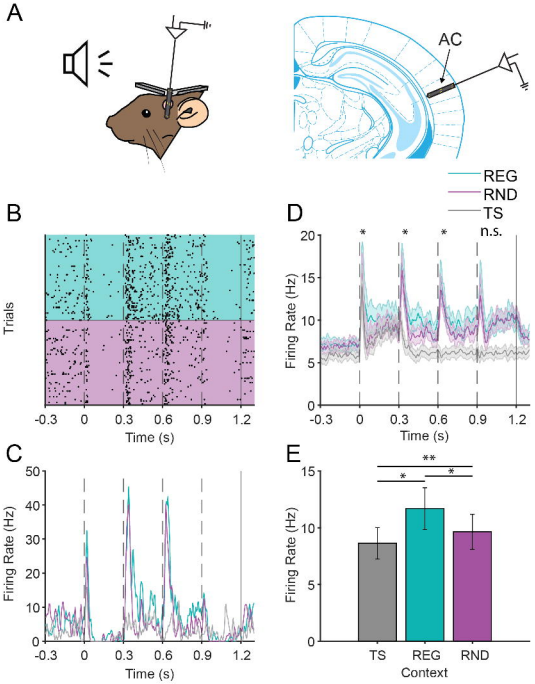
A
AC
REG
RND
TS
B
Trials
-0.3
0
0.3
0.6
0.9
1.2
Time (s)
D
n.s.
Firing Rate (Hz)
Time (s)
C
Firing Rate (Hz)
Time (s)
E
**
*
*
Firing Rate (Hz)
TS
REG
RND
Context

Figure 5

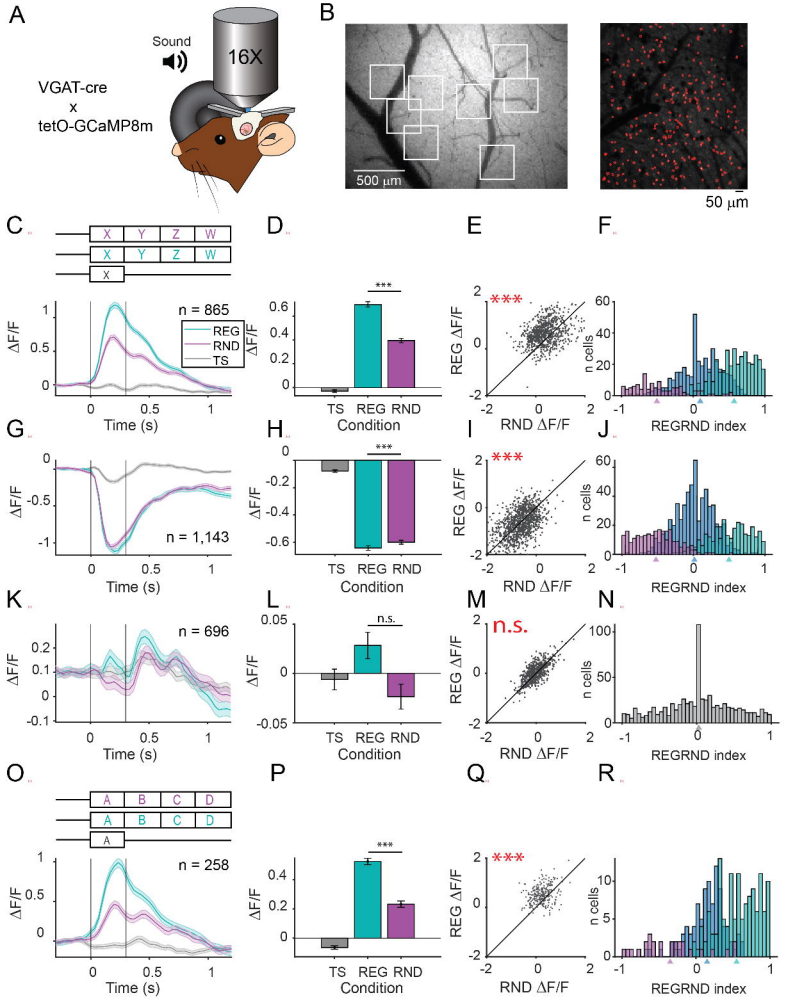
A
Sound
16X
VGAT-cre
x
tetO-GCaMP8m
B
500 µm
50 µm
C
X Y Z W
X Y Z W
X
n = 865
REG
RND
TS
ΔF/F
Time (s)
D
***
ΔF/F
TS REG RND
Condition
E
***
REG ΔF/F
RND ΔF/F
F
n cells
REGRND index
G
n = 1,143
H
I
J
K
n = 696
L
n.s.
M
n.s.
N
O
A B C D
A B C D
A
n = 258
P
Q
R

Figure 6

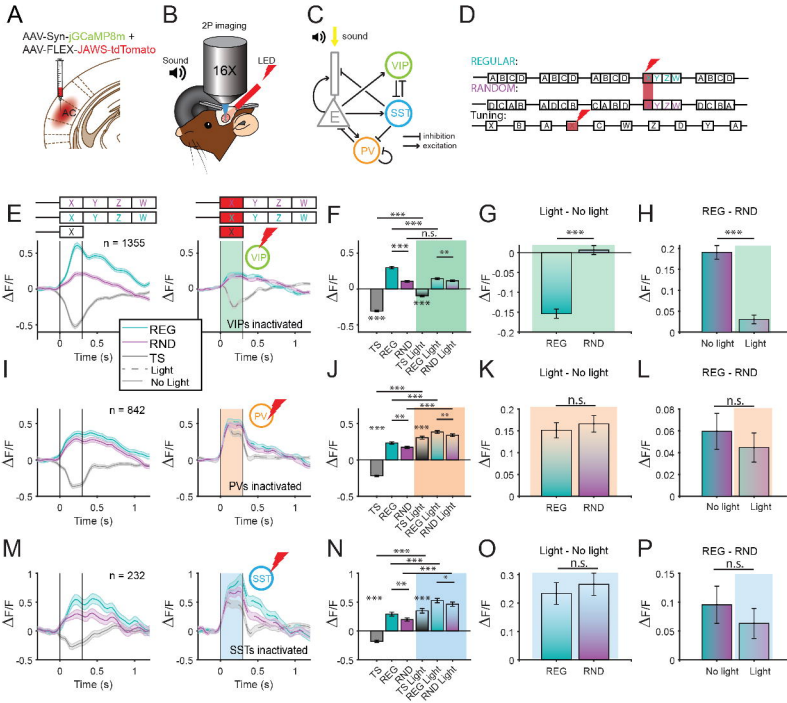
A
AAV-Syn-jGCaMP8m +
AAV-FLEX-JAWS-tdTomato
mC
B
2P imaging
Sound
16X
LED
C
sound
VIP
SST
E
PV
inhibition
excitation
D
REGULAR:
RANDOM:
Tuning:
E
n = 1355
VIPs inactivated
REG
RND
TS
Light
No Light
Time (s)
ΔF/F
F
TS
REG
RND
TS Light
REG Light
RND Light
n.s.
G
Light - No light
REG
RND
H
REG - RND
No light
Light
I
n = 842
PVs inactivated
J
K
L
M
n = 232
SSTs inactivated
N
O
P

Figure 7

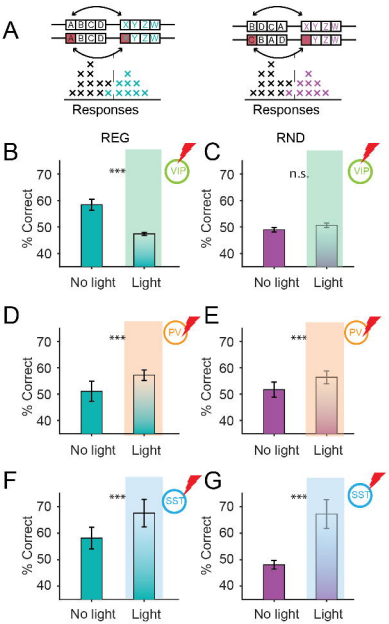
A
Responses
Responses
B
REG
C
RND
D
E
F
G
% Correct
No light
Light
***
n.s.
VIP
PV
SST

Figure 8

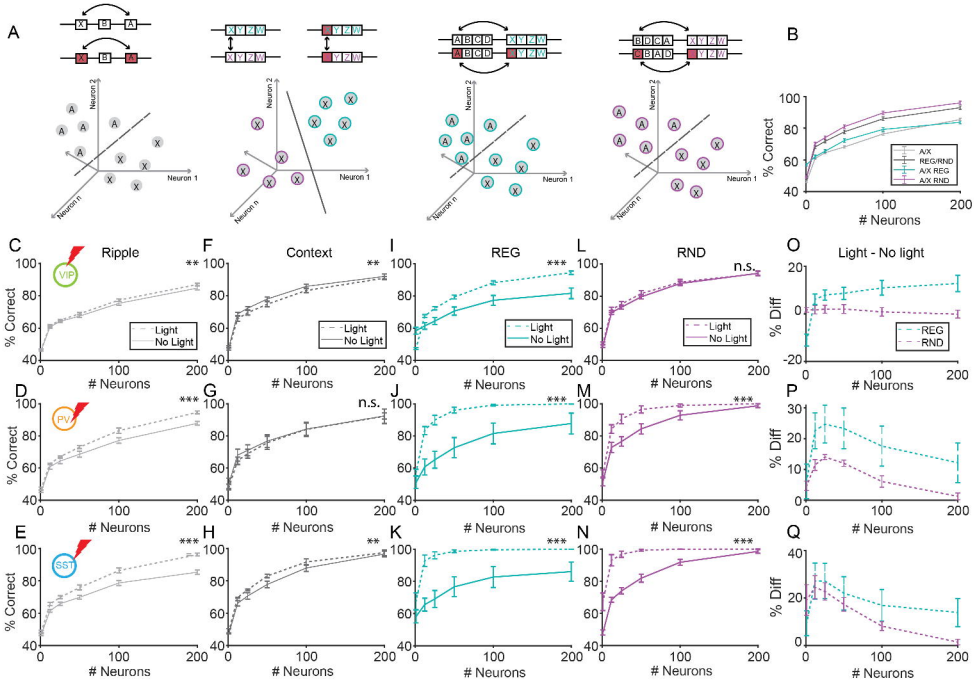
A
B
C
D
E
F
G
H
I
J
K
L
M
N
O
P
Q
Neuron 1
Neuron 2
Neuron n
% Correct
% Diff
# Neurons
A/X
REG/RND
A/X REG
A/X RND
Ripple
Context
REG
RND
Light - No light
VIP
PV
SST
Light
No Light
REG
RND
n.s.
**
***